NASA Technical Memorandum 84281

A Mathematical Model of a Single Main Rotor Helicopter for Piloted Simulation

Peter D. Talbot, Bruce E. Tinling,
William A. Decker, and Robert T. N. Chen

September 1982

National Aeronautics and
Space Administration

NASA Technical Memorandum 84281

A Mathematical Model of a Single Main Rotor Helicopter for Piloted Simulation

Peter D. Talbot
Bruce E. Tinling
William A. Decker
Robert T. N. Chen, Ames Research Center, Moffett,Field, California

National Aeronautics and
Space Administration

Ames Research Center
Moffett Field. California 94035

CONTENTS

TABLES

FIGURES

A MATHEMATICAL MODEL OF A SINGLE MAIN ROTOR HELICOPTER FOR PILOTED SIMULATION

Peter D. Talbot, Bruce E. Tinling, William A. Decker, and Robert T. N. Chen

Ames Research Center

SUMMARY

This report documents a helicopter mathematical model suitable for piloted simulation of flying qualities. The mathematical model is a nonlinear, total force and moment model of a single main rotor helicopter. The model has ten degrees of freedom: six rigid-body, three rotor-flapping, and the rotor rotational degrees of freedom. The rotor model assumes rigid blades with rotor forces and moments radially integrated and summed about the azimuth. The fuselage aerodynamic model uses a detailed representation over a nominal angle of attack and sideslip range of ±15°, and it uses a simplified curve fit at large angles of attack or sideslip. Stabilizing surface aerodynamics are modeled with a lift curve slope between stall limits and a general curve fit for large angles of attack. A generalized stability and control augmentation system is described. Additional computer subroutines provide options for a simplified engine/governor model, atmospheric turbulence, and a linearized six-degree-of-freedom dynamic model for stability and control analysis.

INTRODUCTION

An expanded flying-qualities data base is needed for use in developing design criteria for future helicopters. A safe and cost-effective way to establish such a data base is to conduct exploratory investigations using piloted ground-based simulators, and then to substantiate the results in flight using variable stability research helicopters.

A mathematical model suitable for real-time piloted simulation of single rotor helicopters has been implemented at Ames Research Center. As described in reference 1, simulation models used at Ames Research Center consist of a common core of rigid-body equations and an aerodynamic model that provides the aerodynamic forces and moments. This report documents the equations used in the aerodynamic model.

The report consists of a brief description of the overall model and its components and appendices that detail the equations used in the model and the parameters required to describe a helicopter configuration.

SIMULATION MODEL

The overall arrangement of the simulation model is shown in figure 1. The principal assumptions and considerations employed in developing each element of the model are given in the main body of the report; detailed equations for the forces and moments are given in the appendices. The model elements, denoted T_i in figure 1, are required to achieve transfer of velocities, forces, and moments from

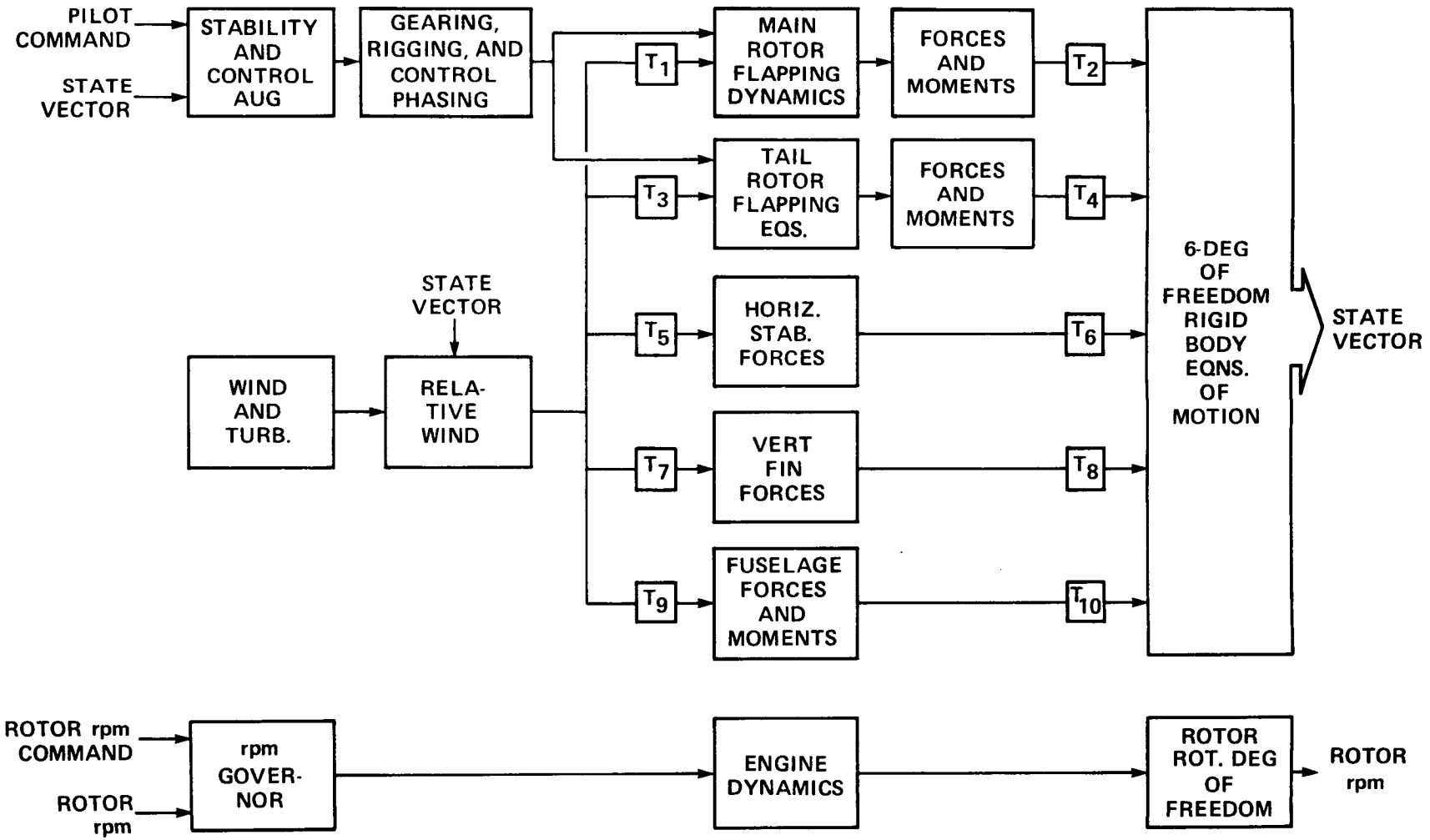

Figure 1.- Block diagram showing principal elements of single rotor helicopter model.

one axis system to another; in some instances, to account for aerodynamic interference effects between model components. These elements are described in the appendices where required.

The notation employed is listed in appendix A, and a description of the various axis systems is given in appendix B. The variable names in the FORTRAN coding for the computer program have been chosen to be easily identifiable from the notation used herein. Through this mnemonic device, equations in the appendix can be identified in the computer program listings.

Main Rotor

The development of the equations describing the dynamics and the forces and moments acting on the main rotor are given in detail in references 2 and 3. This mathematical representation explicitly accounts for the dynamic effect of rotor modes, such as rotor-blade flapping, which can be in a frequency range which is important in studies of flying qualities. For the rotor model described in this report, the flapping dynamics were approximated using a tip-path plane representation.

The flapping equation of motion of the rotor blade was first developed using the following assumptions. The assumptions are similar to those used for the "classical" equations (refs. 4 and 5).

1. The rotor blade was rigid in bending and torsion, and the twist of the blade was linear.

2. The flapping angle and inflow angle were assumed to be small and the analysis utilized a simple strip theory.

3. The effects of the aircraft motion on the blade flapping were limited to those due to the angular acceleration $\dot{p}$ and $\dot{q}$, the angular rate p and q, and the normal acceleration.

4. The reversed flow region was ignored and the compressibility and stall effects disregarded.

5. The inflow was assumed to be uniform and no inflow dynamics were used.

6. The tip-loss factor was assumed to be 1.

The flapping equations of motion explicitly contain the primary design parameters, namely: flapping hinge restraint, hinge offset, blade Lock number, and pitch-flap coupling. The blade flapping in those equations was then approximated by the first harmonic terms with time-varying coefficients, that is,

7. $\beta(t) = a_0(t) - a_1(t)\cos\psi - b_1(t)\sin\psi$.

In the development of the equations for forces and moments, the same set of basic assumptions (1 through 7 above), discussed in conjunction with the development of the tip-path plane dynamic equations, was utilized. Thus, aerodynamically, momentum theory was used in conjunction with the uniform inflow; simple strip theory was utilized and the blade forces were analytically integrated over the radius. Because the reversed flow region and the stall and compressibility effects were ignored, the total rotor forces and moments were again analytically obtained by

summing the contributions, to each blade, that were analytical functions of the azimuth. Because of these assumptions and simplifications, the results of the analysis are valid only for a limited range of flight conditions. Nevertheless, a previous study (ref. 5) has shown that this type of analysis is valid for stability and control investigations of the rotorcraft up to an advance ratio of about 0.3. Also, similar to the development of the tip-path plane dynamic equations, these rotor forces and moments were first obtained in the wind-hub coordinate system. They were then transformed into the hub-body system (see appendix C).

The forces and moments thus developed contain periodic terms; the highest harmonic terms correspond directly to the number of rotor blades. For example, for a three-bladed rotor, the force and moment equations contain only three/revolution harmonic terms, and for a four-bladed rotor, four/revolution harmonic terms. The frequency of these harmonic terms is sufficiently high to be of no interest to handling quality investigations. These terms have therefore been deleted. The resulting force and moment expressions are given in appendix C.

A development to modify these forces and moment equations to include the effects of nonuniform inflow, similar to the development for the flapping equations in references 6 and 7, is in progress. These equations, along with the modified tip-path plane representation given in reference 7 will later supersede those shown in appendix C.

Tail Rotor

The tail rotor was modeled as a teetering rotor without cyclic pitch. For this case, the forces in the wind-hub system may be obtained from the expressions derived for the main rotor by setting the lateral and longitudinal cyclic pitch terms (A_{1_c} and B_{1_c}) equal to zero. Further, since the tail rotor flapping frequency is much higher than that of the main rotor system, the tip-path plane dynamics may be neglected. Thus, for tail rotor applications, the first and second derivatives of the blade-flapping nonrotating coordinates are set equal to zero in the force equations ($\dot{a}_0 = \dot{a}_1 = \dot{b}_1 = 0$ and $\ddot{a}_0 = \ddot{a}_1 = \ddot{b}_1 = 0$). The result is a set of basic quasi-static force expressions similar to those in classical work (refs. 3 and 4).

The local flow at the tail rotor includes the effect of downwash from the main rotor system. The method employed to estimate this downwash and the equations for tail rotor forces are given in appendix D.

Empennage

The lift and drag forces on the vertical fin and horizontal tail are approximated for all angle of attack and sideslip, including rearward flight. Provision is made for the addition of terms due to main rotor-induced velocities at the horizontal tail, and tail rotor velocities at the vertical fin.

The principal assumptions made in developing the expressions for the forces and moments due to the vertical fin and horizontal tail are as follows:

1. The lift and drag forces are applied at the quarter chord of each surface at the spanwise location of the center of area.

2. The airfoil profiles are symmetrical.

3. The lift curve slope prior to stall is given by simple lifting-line theory assuming an elliptical lift distribution with uniform downwash. Corrections are applied for sideslip and for sweep of the vertical fin.

4. Maximum lift coefficient is specified; however, if the lift curve slope is such that this value is not reached at an angle of attack of $\pi/4$, $C_{L_{max}}$ is assumed to occur at this angle of attack.

5. Post stall variation of lift coefficient is based on $C_{L_{max}}$ decreasing by 20% as the angle of attack is increased by 20%, and following a particular variation thereafter to reach zero lift at an angle of attack of $\pi/2$.

6. Lift coefficient in rearward flight is 80% of that in forward flight.

7. The profile drag coefficient varies with angle of attack and reaches a value of 1 when $\alpha = \pm\pi/2$.

8. The induced drag coefficient varies as the square of the calculated lift coefficient.

A typical variation of the lift and drag coefficients for an empennage surface is shown in figure 2. Expressions for calculating the empennage forces and the required transformations for velocities and forces are given in appendix E.

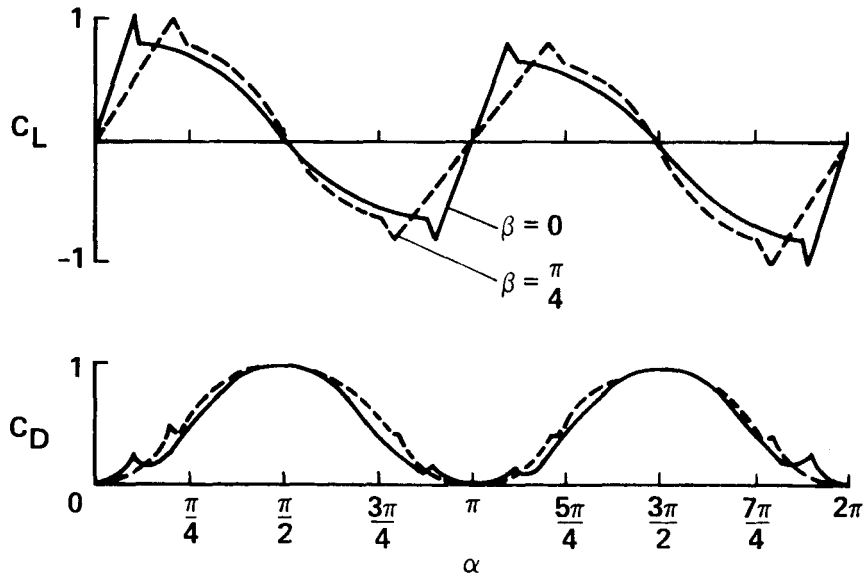

Figure 2.- Typical variation of empennage lift and drag coefficients.

Fuselage

The aerodynamic model of the fuselage must fulfill two requirements. The first is to provide an estimate of the forces and moments at small angles of attack and

sideslip that will be encountered at substantial forward speeds. This provides a representation of the important effects of fuselage aerodynamics on performance and stability at these speeds. The second requirement is to provide a continuous variation of forces and moments over the entire range of angle of attack and sideslip (0° to ±180°) that can be encountered in approach to hovering flight or in hover. Continuity is required to avoid sudden unrealistic linear or angular accelerations in response to a small change in attitude. Accuracy of the model at extreme attitudes is considered to be of secondary importance, since the fuselage forces at these speeds are very small compared to the rotor forces.

A technique has been developed to provide a continuous model by fitting typical variations of the forces and moments through data points obtained at specific widely separated angles of attack and sideslip in a wind tunnel (see ref. 8). However, even this sparse level of test data for the fuselage is typically unavailable and an alternative technique must be employed.

The model employed herein relies on separate representations for angles of attack and sideslip in the range from -15° to 15° and from ±30° to ±180°. Continuity is provided by a linear interpolation for forces and moments in the angle range not covered. The forces and moments for the lower angle range are obtained from test data or from estimates based on data from similar fuselages. The data for the high angle of attack and sideslip range are based on the estimated magnitude and location of the drag force vector when the fuselage is in a 90° cross flow, and on an approximation to its observed variations with attitude from wind-tunnel tests of bodies of revolution.

Details of the procedure for estimating fuselage forces and moments are given in appendix F.

Rotor Rotational Degree of Freedom and RPM Governing

An option is available which provides for a rotational degree of freedom for the rotor. When this option is used, the main rotor and the tail rotor rotational speeds vary according to the current torque requirements and the engine power available. The initial trim conditions establish baseline values of rotor speeds and engine torque. Deviations from these baseline values change the rotor torque requirements and, hence, rotor speed. These changes in speed cause the rpm governor to vary the fuel flow to the engine to change the power to maintain the desired angular rate. A block diagram of the rpm governor is shown in figure 3. Further details of the dynamic model for this degree of freedom and the rpm governor are given in appendix G.

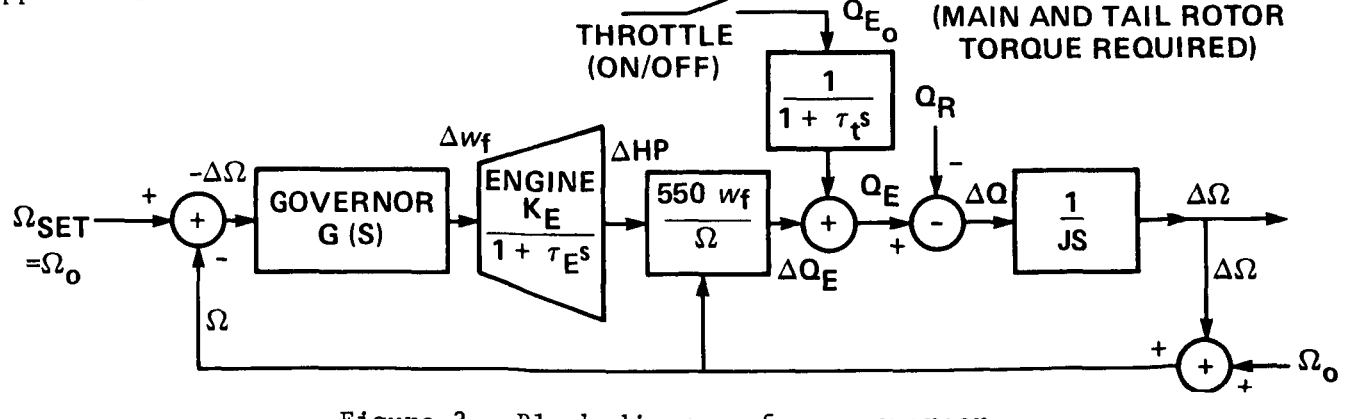

Figure 3.- Block diagram of rpm governor.

Control Systems

The helicopter model has a generalized control system that accepts inputs from the pilot, facilitates control augmentation and stability augmentation, and provides for mechanical control mixing or phasing of the cyclic inputs. A block diagram of this system is shown in figure 4. The control augmentation system employs a

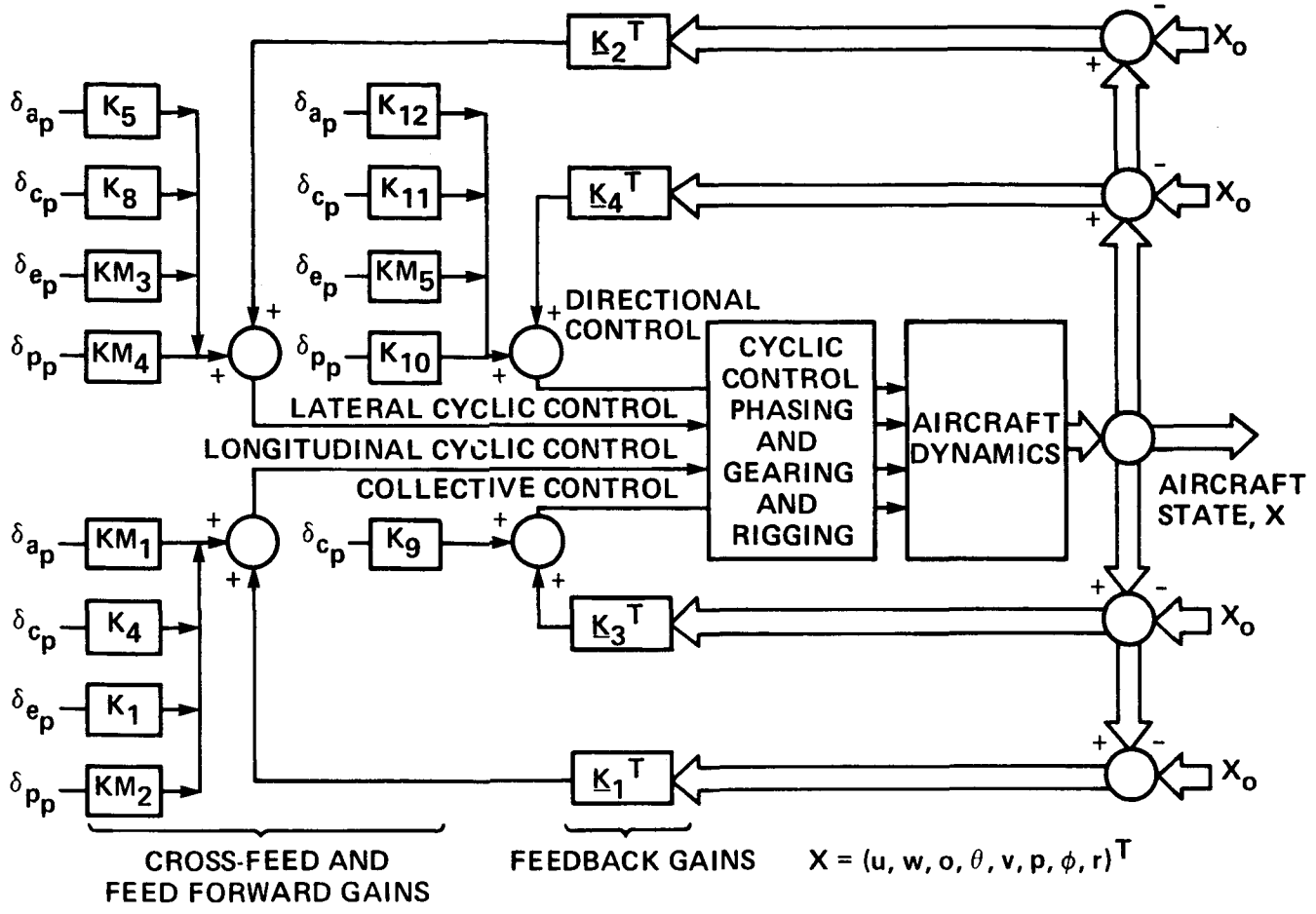

Figure 4.- Structure of control system model.

structure that permits implementation of crossfeeds from each of the four cockpit controls; namely, longitudinal and lateral cyclic stick, collective stick, and directional pedals. The feedback gain structure of the stability augmentation system permits feedback proportional to any element of the state vector to each of the four controls. The entire control structure also facilitates gain scheduling as functions of the flight parameters, such as airspeed.

Details concerning the zero position and sign convention of the cockpit controls and the mechanical cyclic control phasing logic are given in appendix H.

Atmospheric Turbulence

The representation of atmospheric turbulence is based on the Dryden model and is described in MIL-F-8785B (ref. 9). The inputs required for this model are the aircraft velocity relative to the air mass, the turbulence scale lengths, and the rms

gust levels. For this representation, scale length and the wind velocity can be specified as functions of altitude. The rms gust levels are dependent upon wind velocity.

Linearized Six-Degree-of-Freedom Model

A computer subroutine is available that generates the coefficients of a linear, first-order set of differential equations that represents the rigid body dynamics of the helicopter for small perturbations from a fixed operating point. The principal assumption necessary to generate this linear set of equations is that the helicopter initial angular rates are zero. The differential equations are of the form:

$$\dot{x} = [F]x + [G]\delta$$

where x represents perturbations from trim of the state variables u, w, q, θ, v, p, ϕ, and r; and δ represents the control displacements from trim $\Delta\delta_e$, $\Delta\delta_c$, $\Delta\delta_a$, and $\Delta\delta_p$. The generation of the F and G matrices and a description of each element is given in appendix I.

APPENDIX A

NOTATION

a	blade lift-curve slope, per rad
a_o	blade coning angle measured from hub plane in the hub-wind axes system, rad
a_1	longitudinal first-harmonic flapping coefficient measured from the hub plane in the wind-hub axes system, rad
a_{1_s}	longitudinal first-harmonic flapping coefficient measured from the hub plane in the hub-body axes system, rad
A_{1_c}	lateral cyclic pitch measured from hub plane in the wind-wub axes system, rad
A_{1_s}	lateral cyclic pitch measured from hub plane in the hub-body axes system, rad
AR	aspect ratio, $\text{span}^2/\text{area}$
b_1	lateral first-harmonic flapping coefficient measured from hub plane in the wind-hub axes system, rad
b_{1_s}	lateral first-harmonic flapping coefficient measured from hub plane in the hub-body axes system, rad
BL	lateral distance (buttline) in the fuselage axes system, m (ft)
B_{1_c}	longitudinal cyclic pitch measured from hub plane in the wind-hub axes system, rad
B_{1_s}	longitudinal cyclic pitch measured from hub plane in the hub-body axes system, rad
c	blade chord, m (ft)
c_n	control gearing constants, n = 1 to 8
$C_{A_{1_s}}$, $C_{B_{1_s}}$	cyclic control rigging constants, rad
C_D	drag coefficient
C_L	lift coefficient
C_{L_M}	maximum lift coefficient
C_T	rotor thrust coefficient, $T/\rho(\pi R^2)(\Omega R)^2$
D	drag force, N (lb)

$\tilde{D}$	damping matrix in flapping differential equations
e	flapping hinge offset, m(ft)
g	gravitational acceleration, m/sec^2 (ft/sec^2)
H	rotor force normal to shaft, positive downwind, N (lb)
i_F	incidence of vertical fin, positive for leading edge to the left, rad
i_{HS}	incidence of horizontal stabilizer, positive for leading edge up, rad
i_s	forward tilt of rotor shaft w.r.t. fuselage, positive forward, rad
I_β	rotor blade moment of inertia about flapping hinge, $kg-m^2$ ($slug-ft^2$)
J	rotor moment of inertia about shaft
$k_{v_{TR}}$	factor to account for fraction of vertical tail in tail rotor wake
K_β	flapping spring constant, N-m/rad (lb-ft/rad)
K_1	pitch-flap coupling ratio, $\triangleq \tan \delta_3$
$\tilde{K}$	spring matrix in flapping differential equations
ℓ	fuselage rolling moment, n-m (ft-lb)
L	fuselage lift, N (lb)
L, M, N	rolling moment, pitching moment, and yawing moment, respectively, N-m (ft-lb)
m	rotor blade mass, kg (slugs)
M_β	blade weight moment about flapping hinge, N-m (lb-ft)
n_b	number of blades
p, q, r	roll, pitch, and yaw rates in the body-c.g. axes system, rad/sec
p_B, q_B, r_B	roll, pitch, and yaw rates in the body-c.g. axes system relative to the air mass, rad/sec
p_H, q_H, r_H	roll, pitch, and yaw rates in the hub-body axes system, rad/sec
P	ratio of flapping frequency to rotor system angular velocity
q	dynamic pressure, $\frac{1}{2}\rho V^2$, N/m^2 (lb/ft^2)

Q	torque, N-m (ft-lb)
R	rotor radius, m (ft)
s	Laplace variable
S	area of stabilizing surface, m^2 (ft^2)
STA	longitudinal location in the fuselage axes system, m (ft)
T	thrust, N (lb)
u, v, w	longitudinal, lateral, and vertical velocities in the body-c.g. system of axes, m/sec (ft/sec)
u_B, v_B, w_B	longitudinal, lateral, and vertical velocities relative to the air mass in the body-c.g. system of axes, m/sec (ft/sec)
u_H, v_H, w_H	longitudinal, lateral, and vertical velocities relative to the air mass in the air mass in the hub-body system of axes, m/sec (ft/sec)
v_i	main rotor induced velocity at rotor disk, m/sec (ft/sec)
w_f	fuel flow rate, N/hr (lb/hr)
WL	vertical location in the fuselage axes system, m (ft)
X, Y, Z	longitudinal, lateral, and vertical forces in the body-c.g. axes system, N (lb)
α	stabilizing surface angle of attack, rad
α_s	angle of attack for stall, rad
β_w	rotor sideslip angle, rad
γ	blade Lock number, $\rho acR^4/I_\beta$
δ	equivalent rotor blade profile drag coefficient
δ_a	lateral cyclic stick movement, positive to right, cm (in.)
δ_c	collective control input, positive up, cm (in.)
δ_e	longitudinal cyclic stick movement, positive aft, cm (in.)
δ_p	pedal movement, positive right, cm (in.)
ε	hinge offset ratio, e/R
η	stabilizing surface lift efficiency factor

θ Euler pitch angle, rad

θ_o blade root collective pitch, rad

θ_t total blade twist (root minus tip incidence), rad

λ inflow ratio $\triangleq \frac{w_H}{\Omega} - \frac{C_T}{2(\mu^2 + \lambda^2)^{1/2}}$

Λ sweepback angle of fin, rad

μ rotor advance ratio, $\frac{\sqrt{u_H^2 + v_H^2}}{\Omega R}$

ρ air desntiy, kg/m^3 ($slugs/ft^3$)

σ rotor solidity ratio, blade area/disk area

τ time constant

ϕ Euler roll angle, rad

Ω rotor angular velocity, rad/sec

Subscripts:

B body-c.g. axes system relative to air mass

c.g. center of gravity

E engine

f fuselage

F vertical fin

H hub-body axes system, hub location

HS horizontal stabilizer

i induced

MR main rotor

p pilot input

t throttle

TR tail rotor

W hub-wind system of axes

APPENDIX B

AXIS SYSTEMS

Hub Wind

The hub-wind axis system is used in the calculation of rotor forces and moments. The origin of the system is the rotor hub, and the T (thrust) axis is aligned with the rotor shaft. The H_W (horizontal) axis is aligned with the component of relative wind normal to the shaft axis, and the Y_W (side force) axis completes the right-handed orthogonal set. This axis system is shown in figure B-1 along with the components of the relative wind.

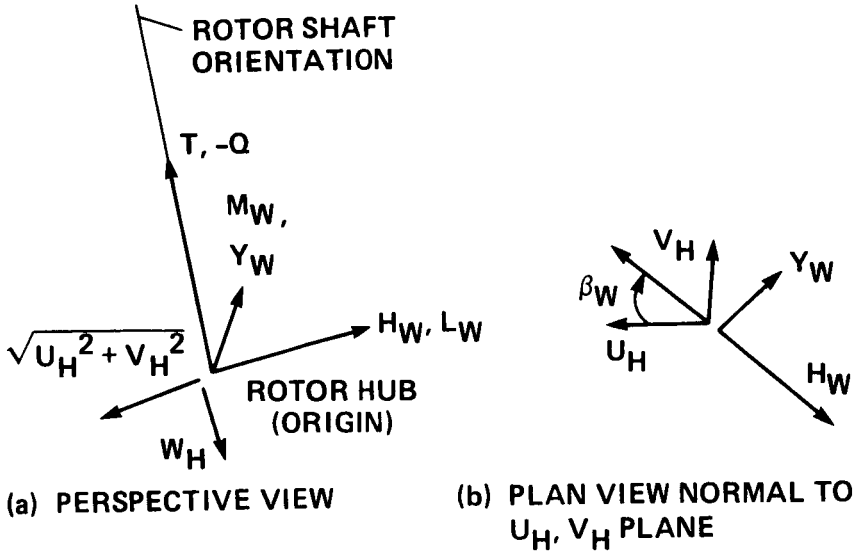

Figure B-1.- The hub-wind axis system with main rotor force, moment, and velocity components defined.

Hub Body

The hub-body system coincides with the hub-wind system when the sideslip angle β_W is zero. Thus, the T axis is aligned with the shaft axis, and the force H_R lies in the $x_B - z_B$ plane (see fig. B-2).

Body Center of Gravity

All forces and moments are expressed relative to the body-c.g. system for use in the six-degrees-of-freedom rigid body equations of motion. This axis system has its origin at the center of gravity with the x axis aligned with the longitudinal axis of the helicopter, and the z axis lying on the plane of symmetry (see fig. B-2).

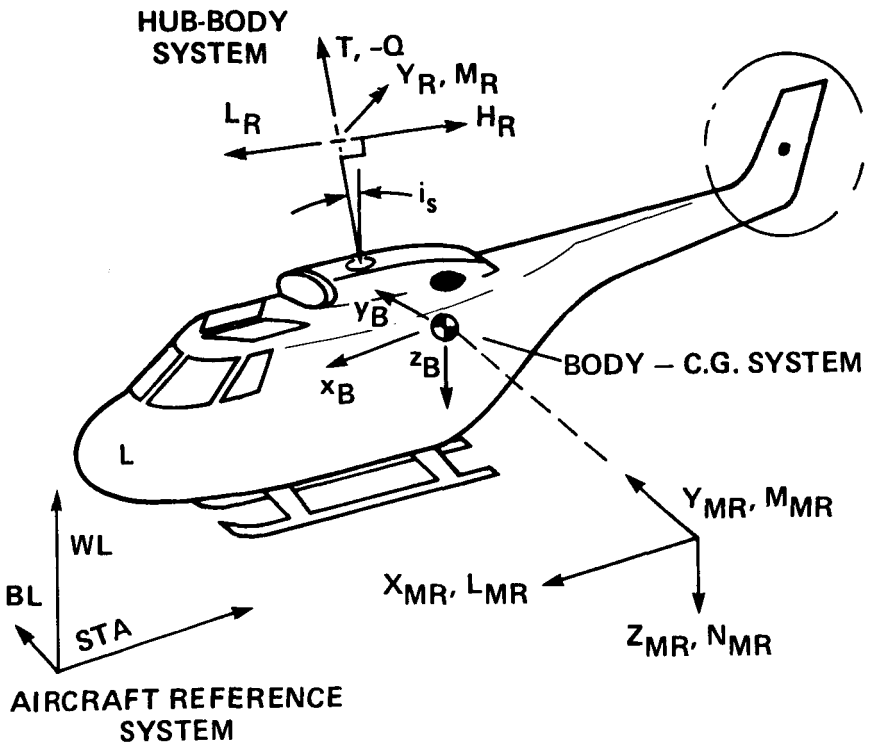

Figure B-2.- Hub-body, aircraft reference and body-c.g. axis systems.

Aircraft Reference

The aircraft reference axes are used to locate all force and moment generating components and the center of gravity. The aircraft reference axes are parallel to the body-c.g. axes. The axis origin is typically located ahead and below the aircraft at some arbitrary point within the plane of symmetry. Stations are measured positive aft along the longitudinal axis. Buttlines are lateral distances, positive to the pilot's right. Waterlines are measured vertically, positive upward (see fig. B-2).

Local Wind

The local-wind axes systems are employed for calculation of lift and drag forces on the empennage and on the fuselage. For each empennage surface, the origin is at the quarter point of the mean aerodynamic chord, and the lift force is normal to the relative wind and to a spanwise line passing through the quarter chord point.

APPENDIX C

MAIN ROTOR FLAPPING DYNAMICS AND FORCE AND MOMENT CALCULATION

The derivation of the tip-path plane dynamic equation is given in detail in reference 2. For the nonteetering N-bladed rotor, the tip-path plane dynamic equations are as follows:

$$\ddot{\underline{a}} + \tilde{D}\underline{a} + \tilde{K}\underline{a} = \tilde{f}$$

$$\tilde{D} = \Omega \begin{bmatrix} \frac{\gamma}{2}\left(\frac{1}{4} - \frac{2}{3}\varepsilon + \frac{\varepsilon^2}{2}\right) & 0 & -\frac{\gamma\mu}{4}\left(\frac{1}{3} - \varepsilon + \varepsilon^2\right) \\ 0 & \frac{\gamma}{2}\left(\frac{1}{4} - \frac{2}{3}\varepsilon + \frac{\varepsilon^2}{2}\right) & 2 \\ -\frac{\gamma\mu}{2}\left(\frac{1}{3} - \varepsilon + \varepsilon^2\right) & -2 & \frac{\gamma}{2}\left(\frac{1}{4} - \frac{2}{3}\varepsilon + \frac{\varepsilon^2}{2}\right) \end{bmatrix}$$

$$\tilde{K} = \Omega^2 \begin{bmatrix} P^2 + \frac{\gamma K_1 \mu^2}{4}\left(\frac{1}{2} - \varepsilon + \frac{\varepsilon^2}{2}\right) & -\frac{\gamma\mu}{4}\left(\frac{\varepsilon}{2} - \varepsilon^2\right) & -\frac{\gamma K_1 \mu}{4}\left(\frac{2}{3} - \varepsilon\right) \\ -\frac{\gamma\mu}{2}\left(\frac{1}{3} - \frac{\varepsilon}{2}\right) & P^2 - 1 + \frac{\gamma K_1 \mu^2}{8}\left(\frac{1}{2} - \varepsilon + \frac{\varepsilon^2}{2}\right) & \frac{\gamma}{2}\left(\frac{1}{4} - \frac{2}{3}\varepsilon + \frac{\varepsilon^2}{2}\right) + \frac{\gamma\mu^2}{8}\left(\frac{1}{2} - \varepsilon + \frac{\varepsilon^2}{2}\right) \\ -\frac{\gamma K_1 \mu}{2}\left(\frac{2}{3} - \varepsilon\right) & -\frac{\gamma}{2}\left(\frac{1}{4} - \frac{2}{3}\varepsilon + \frac{\varepsilon^2}{2}\right) + \frac{\gamma\mu^2}{8}\left(\frac{1}{2} - \varepsilon + \frac{\varepsilon^2}{2}\right) & P^2 - 1 + \frac{3}{8}\gamma K_1 \mu^2\left(\frac{1}{2} - \varepsilon + \frac{\varepsilon^2}{2}\right) \end{bmatrix}$$

$$\tilde{f} = \Omega^2 \begin{bmatrix} -\frac{M_\beta}{I_\beta \Omega^2} + \frac{\gamma}{2}\left[\left(\frac{1}{4} - \frac{\varepsilon}{3}\right) + \frac{\mu^2}{2}\left(\frac{1}{2} - \varepsilon + \frac{\varepsilon^2}{2}\right)\right]\theta_0 - \frac{\gamma}{2}\left[\mu\left(\frac{1}{3} - \frac{\varepsilon}{2}\right)\right] B_{1c} + \frac{\gamma}{2}\left[\left(\frac{1}{5} - \frac{\varepsilon}{4}\right) + \frac{\mu^2}{2}\left(\frac{1}{3} - \frac{\varepsilon}{2}\right)\right]\theta_t + \frac{\gamma}{2}\left(\frac{1}{3} - \frac{\varepsilon}{2}\right)\lambda \\ \quad + \frac{\gamma}{8}\mu\left(\frac{2}{3} - \varepsilon\right)\left(\frac{P_H}{\Omega}\cos\beta_w + \frac{q_H}{\Omega}\sin\beta_w\right) \\ -2\left(1 + \frac{eM_\beta}{gI_\beta}\right)\left(\frac{P_H}{\Omega}\cos\beta_w + \frac{q_H}{\Omega}\sin\beta_w\right) + \left(\frac{\dot{P}_H}{\Omega^2}\sin\beta_w - \frac{\dot{q}_H}{\Omega^2}\cos\beta_w\right) + \frac{\gamma}{2}\left[\left(\frac{1}{4} - \frac{\varepsilon}{3}\right) + \frac{\mu^2}{4}\left(\frac{1}{2} - \varepsilon + \frac{\varepsilon^2}{2}\right)\right] A_{1c} \\ \quad + \frac{\gamma}{2}\left(\frac{1}{4} - \frac{\varepsilon}{3}\right)\left(\frac{P_H}{\Omega}\sin\beta_w - \frac{q_H}{\Omega}\cos\beta_w\right) \\ -2\left(1 + \frac{eM_\beta}{gI_\beta}\right)\left(\frac{P_H}{\Omega}\sin\beta_w - \frac{q_H}{\Omega}\cos\beta_w\right) - \left(\frac{\dot{P}_H}{\Omega^2}\cos\beta_w + \frac{\dot{q}_H}{\Omega^2}\sin\beta_w\right) - \frac{\gamma}{2}\mu\left(\frac{2}{3} - \varepsilon\right)\theta_0 - \frac{\gamma\mu}{2}\left(\frac{1}{2} - \frac{2\varepsilon}{3}\right)\theta_t \\ \quad + \frac{\gamma}{2}\left[\left(\frac{1}{4} - \frac{\varepsilon}{3}\right) + \frac{3\mu^2}{4}\left(\frac{1}{2} - \varepsilon + \frac{\varepsilon^2}{2}\right)\right] B_{1c} - \frac{\gamma\mu}{2}\left(\frac{1}{2} - \varepsilon + \frac{\varepsilon^2}{2}\right)\lambda - \frac{\gamma}{2}\left(\frac{1}{4} - \frac{\varepsilon}{3}\right)\left(\frac{P_H}{\Omega}\cos\beta_w + \frac{q_H}{\Omega}\sin\beta_w\right) \end{bmatrix} \qquad (1)$$

where

$$P^2 = 1 + \frac{K_\beta}{I_\beta \Omega^2} + \frac{eM_\beta}{gI_\beta} + \frac{\gamma K_1}{8}\left(1 - \frac{4}{3}\varepsilon\right)$$

and

$$\underline{a} = (a_0, a_1, b_1)^T$$

For a two-bladed teetering rotor, the tip-path plane representation loses its physical meaning. However, if the approximation for blade flapping is employed, that is,

$$\beta(t) = a_0(t) - a_1(t)\cos\psi - b_1(t)\sin\psi$$

then a_0 is treated as a preset constant. The coefficients $a_1(t)$ and $b_1(t)$ can then be solved for by setting $\varepsilon = \dot{a}_0 = \ddot{a}_0 = 0$ in equation (1).

The force and moment expressions, with the harmonic terms dropped that correspond to the number of rotor blades are given below. A derivation of these equations is given in reference 2.

$$T_{MR} = \frac{n_b}{2}\rho acR(\Omega R)^2\left\{\frac{1}{2}(1-\varepsilon^2)\lambda + \theta_0\left[\frac{1}{3} + \frac{\mu^2}{2}(1-\varepsilon)\right] + \theta_t\left[\frac{1}{4} + \frac{\mu^2}{4}(1-\varepsilon^2)\right]\right.$$

$$- \frac{\mu}{2}(1-\varepsilon^2)(B_{1c} - K_1 b_1) - a_0\left[\frac{1}{3} + \frac{\mu^2}{2}(1-\varepsilon)\right]K_1 + a_1\left[\frac{\mu}{2}\varepsilon(1-\varepsilon)\right] - \frac{\dot{a}_0}{\Omega}\left(\frac{1}{3} - \frac{\varepsilon}{2}\right)$$

$$\left. + \frac{\dot{b}_1}{\Omega}\left[\frac{\mu}{4}(1-\varepsilon)^2\right] + \frac{\mu}{4}(1-\varepsilon^2)\left(\frac{p_H}{\Omega}\cos\beta_w + \frac{q_H}{\Omega}\sin\beta_w\right)\right\} - \frac{n_b M_\beta}{g}\ddot{a}_0$$

$$H_W = \frac{n_b}{2} \rho acR(\Omega R)^2 \left(\frac{\delta\mu}{2a} (1 - \varepsilon^2) - \frac{1}{4} (\theta_0 - K_1 a_0) \left[2\lambda\mu(1 - \varepsilon) - \mu(1 - \varepsilon)^2 \frac{\dot{a}_0}{\Omega} \right.\right.$$

$$\left. - \left(\varepsilon - \frac{2}{3}\right)\left(\frac{\dot{b}_1}{\Omega} - a_1\right) - \frac{2}{3} a_1 + \frac{2}{3}\left(\frac{p_H}{\Omega} \cos\beta_w + \frac{q_H}{\Omega} \sin\beta_w\right)\right]$$

$$- \frac{\theta_t}{4} \left[\mu\lambda(1 - \varepsilon^2) + \frac{\dot{a}_0}{\Omega} \mu\left(\varepsilon - \frac{2}{3}\right) - 2\left(\frac{\varepsilon}{3} - \frac{1}{4}\right)\left(\frac{\dot{b}_1}{\Omega} - a_1\right) - \frac{a_1}{2} \right.$$

$$\left. + \frac{1}{2}\left(\frac{p_H}{\Omega} \cos\beta_w + \frac{q_H}{\Omega} \sin\beta_w\right)\right] + \frac{1}{4} (A_{1c} - K_1 a_1) \left[- \frac{b_1 \mu}{4} (1 - \varepsilon^2) \right.$$

$$\left. + \frac{1}{4} \mu(1 - \varepsilon)^2 \left(\frac{\dot{a}_1}{\Omega} + b_1\right) + \frac{2}{3} a_0 + \frac{\mu}{4} (1 - \varepsilon^2)\left(- \frac{p_H}{\Omega} \sin\beta_w + \frac{q_H}{\Omega} \cos\beta_w\right)\right]$$

$$+ \frac{1}{4} (B_{1c} - K_1 b_1) \left[\frac{3}{4} \mu(1 - \varepsilon)^2 \left(\frac{\dot{b}_1}{\Omega} - a_1\right) + (1 - \varepsilon^2)\left(\lambda - \frac{a_1 \mu}{4}\right) + \left(\varepsilon - \frac{2}{3}\right) \frac{\dot{a}_0}{\Omega} \right.$$

$$\left. + \frac{3\mu}{4} (1 - \varepsilon^2) \left(\frac{p_H}{\Omega} \cos\beta_w + \frac{q_H}{\Omega} \sin\beta_w\right)\right] + \frac{1}{4} \left\{ \varepsilon(1 - \varepsilon) \left(\frac{\dot{b}_1}{\Omega} - a_1\right) 4\lambda \right.$$

$$- (1 - \varepsilon^2)\left[2\lambda \left(\frac{\dot{b}_1}{\Omega} - a_1\right) - a_1 \lambda \right] - \left(\frac{2}{3} - \varepsilon\right)\left[a_1 \frac{\dot{a}_0}{\Omega} + a_0 \left(\frac{\dot{a}_1}{\Omega} + b_1\right)\right]$$

$$- \frac{2a_0}{3} \left(- \frac{p_H}{\Omega} \sin\beta_w + \frac{q_H}{\Omega} \cos\beta_w\right) - \left[2(1 - \varepsilon^2)\lambda - 4\left(\frac{1}{3} - \frac{\varepsilon}{2}\right) \frac{\dot{a}_0}{\Omega} \right] \left(\frac{p_H}{\Omega} \cos\beta_w \right.$$

$$\left. + \frac{q_H}{\Omega} \sin\beta_w\right) + 4 \frac{\dot{a}_0}{\Omega} \left(\frac{\dot{b}_1}{\Omega} - a_1\right)\left(\frac{1}{3} - \varepsilon + \varepsilon^2\right) \Big\} + \frac{\mu}{4} \left\{ \varepsilon(1 - \varepsilon) \left[a_1 \left(\frac{\dot{b}_1}{\Omega} - a_1\right) \right.\right.$$

$$\left. + b_1 \left(\frac{\dot{a}_1}{\Omega} + b_1\right)\right] + \frac{1}{4} (1 - \varepsilon)^2 \left[b_1 \left(\frac{\dot{a}_1}{\Omega} + b_1\right) + a_1 \left(\frac{\dot{b}_1}{\Omega} - a_1\right)\right]$$

$$- \frac{1}{2} (1 - \varepsilon^2)\left[a_1 \left(\frac{\dot{b}_1}{\Omega} - a_1\right) + b_1 \left(\frac{\dot{a}_1}{\Omega} + b_1\right) - 2a_0^2 - \frac{b_1^2}{2} - \frac{3}{2} a_1^2 \right]$$

$$\left. \left. - \frac{a_1}{4} (1 - \varepsilon^2) \left(\frac{p_H}{\Omega} \cos\beta_w + \frac{q_H}{\Omega} \sin\beta_w\right) - \frac{b_1}{4} (1 - \varepsilon^2)\left(- \frac{p_H}{\Omega} \sin\beta_w + \frac{q_H}{\Omega} \cos\beta_w\right) \right\} \right)$$

$$Y_W = \frac{n_b}{2}\rho acR(\Omega R)^2\Bigg(-\frac{1}{4}(\theta_0 - K_1 a_0)\Bigg\{\Bigg[\Big(\varepsilon - \frac{2}{3}\Big)\Big(\frac{\dot{a}_1}{\Omega} + b_1\Big) - \frac{2}{3}b_1\Bigg] + 3a_0(1-\varepsilon^2)\mu$$
$$- 2b_1(1-\varepsilon)\mu^2 - \frac{2}{3}\Big(-\frac{p_H}{\Omega}\sin\beta_w + \frac{q_H}{\Omega}\cos\beta_w\Big)\Bigg\} - \frac{\theta_t}{4}\Bigg\{\Bigg[\Big(\frac{2\varepsilon}{3} - \frac{1}{2}\Big)\Big(\frac{\dot{a}_1}{\Omega} + b_1\Big) - \frac{b_1}{2}\Bigg]$$
$$+ 2a_0\mu - b_1(1-\varepsilon^2)\mu^2 - \frac{1}{2}\Big(-\frac{p_H}{\Omega}\sin\beta_w + \frac{q_H}{\Omega}\cos\beta_w\Big)\Bigg\}$$
$$- \frac{1}{4}(A_{1c} - K_1 a_1)\Bigg\{\Bigg[\Big(\varepsilon - \frac{2}{3}\Big)\frac{\dot{a}_0}{\Omega} + \lambda(1-\varepsilon^2)\Bigg] + \mu\Bigg[\frac{5a_1}{4}(1-\varepsilon^2)$$
$$+ \frac{1}{4}(1-\varepsilon)^2\Big(\frac{\dot{b}_1}{\Omega} - a_1\Big)\Bigg] + \frac{\mu}{4}(1-\varepsilon^2)\Big(\frac{p_H}{\Omega}\cos\beta_w + \frac{q_H}{\Omega}\sin\beta_w\Big)\Bigg\}$$
$$- \frac{1}{4}(B_{1c} - K_1 b_1)\Bigg\{-\frac{2}{3}a_0 + \mu\Bigg[\frac{7}{4}b_1(1-\varepsilon^2) + \frac{1}{4}(1-\varepsilon)^2\Big(\frac{\dot{a}_1}{\Omega} + b_1\Big)$$
$$+ \frac{1}{4}\Big(-\frac{p_H}{\Omega}\sin\beta_w + \frac{q_H}{\Omega}\cos\beta_w\Big)\Bigg] - \mu^2[2a_0(1-\varepsilon)]\Bigg\}$$
$$- \frac{1}{4}\Bigg\{4\Big(\frac{1}{3} - \varepsilon + \varepsilon^2\Big)\frac{\dot{a}_0}{\Omega}\Big(\frac{\dot{a}_1}{\Omega} + b_1\Big) - 2\lambda(1-\varepsilon)^2\Big(\frac{\dot{a}_1}{\Omega} + b_1\Big)$$
$$+ \frac{2a_0}{3}\Big(\frac{p_H}{\Omega}\cos\beta_w + \frac{q_H}{\Omega}\sin\beta_w\Big) + 2a_0\Big(\frac{1}{3} - \frac{\varepsilon}{2}\Big)\Big(\frac{\dot{b}_1}{\Omega} - a_1\Big) - 2b_1\Bigg[\frac{\lambda}{2}(1-\varepsilon^2)$$
$$- \frac{\dot{a}_0}{\Omega}\Big(\frac{1}{3} - \frac{\varepsilon}{2}\Big)\Bigg] + \Bigg[4\Big(\frac{1}{3} - \frac{\varepsilon}{2}\Big)\frac{\dot{a}_0}{\Omega} - 2(1-\varepsilon^2)\lambda\Bigg]\Big(-\frac{p_H}{\Omega}\sin\beta_w + \frac{q_H}{\Omega}\cos\beta_w\Big)\Bigg\}$$
$$- \frac{\mu}{4}\Bigg[6a_0\lambda(1-\varepsilon) - \frac{a_1 b_1}{2}(1-\varepsilon^2) - 3(1-\varepsilon)^2 a_0\frac{\dot{a}_0}{\Omega}$$
$$- \frac{7}{4}(1-\varepsilon)^2 a_1\Big(\frac{\dot{a}_1}{\Omega} + b_1\Big) - \frac{5}{4}b_1(1-\varepsilon^2)\Big(\frac{p_H}{\Omega}\cos\beta_w + \frac{q_H}{\Omega}\sin\beta_w\Big)$$
$$- \frac{7}{4}a_1(1-\varepsilon^2)\Big(-\frac{p_H}{\Omega}\sin\beta_w + \frac{q_H}{\Omega}\cos\beta_w\Big) - \frac{5}{4}(1-\varepsilon)^2 b_1\Big(\frac{\dot{b}_1}{\Omega} - a_1\Big)\Bigg]$$
$$- \mu^2[a_0 a_1(1-\varepsilon)]\Bigg)$$

$$M_W = \frac{n_b}{2}\Bigg[K_\beta a_1 - \frac{eM_\beta}{g}(\ddot{a}_1 + 2\dot{b}_1\Omega - a_1\Omega^2)\Bigg] - \frac{n_b}{2}I_\beta\Omega^2\gamma\varepsilon\Bigg\{-\Bigg[\frac{1}{6} + \frac{\mu^2}{8}(1-\varepsilon)\Bigg](A_{1c} - K_1 a_1)$$
$$- \frac{\mu}{4}(1-\varepsilon^2)a_0 + \frac{\mu^2}{8}(1-\varepsilon)b_1 + \Big(\frac{1}{6} - \frac{\varepsilon}{4}\Big)\Big(\frac{\dot{a}_1}{\Omega} + b_1\Big) + \frac{1}{6}\Big(-\frac{p_H}{\Omega}\sin\beta_w + \frac{q_H}{\Omega}\cos\beta_w\Big)\Bigg\}$$

$$L_W = \frac{n_b}{2}\left[K_\beta b_1 - \frac{eM_\beta}{g}\left(\ddot{b}_1 - 2\dot{a}_1\Omega - b_1\Omega^2\right)\right] - \frac{n_b}{2} I_\beta \Omega^2 \gamma\varepsilon \left\{\frac{\mu}{2}(1-\varepsilon^2)(\theta_0 - K_1 a_0)\right.$$

$$-\left[\frac{1}{6} + \frac{3}{8}\mu^2(1-\varepsilon)\right](B_{1c} - K_1 b_1) + \frac{\mu}{3}\theta_t + \frac{\mu}{2}(1-\varepsilon)\lambda + \frac{\mu^2}{8}(1-\varepsilon)a_1$$

$$\left. - \frac{\mu}{4}(1-\varepsilon)^2\frac{\dot{a}_0}{\Omega} + \left(\frac{1}{6} - \frac{\varepsilon}{4}\right)\left(\frac{\dot{b}_1}{\Omega} - a_1\right) + \frac{1}{6}\left(\frac{p_H}{\Omega}\cos\beta_w + \frac{q_H}{\Omega}\sin\beta_w\right)\right\}$$

$$Q = \frac{n_b}{2}\rho acR^2(\Omega R)^2\left(\frac{\delta}{4a}\left[1 + (1-\varepsilon^2)\mu^2\right] - (\theta_0 - K_1 a_0)\left[\frac{\lambda}{3} + \left(\frac{\varepsilon}{3} - \frac{1}{4}\right)\frac{\dot{a}_0}{\Omega} + \frac{\mu}{6}\left(\frac{\dot{b}_1}{\Omega}\right)\right.\right.$$

$$- \frac{\mu\varepsilon}{4}\left(\frac{\dot{b}_1}{\Omega} - a_1\right) + \frac{\mu}{6}\left(\frac{p_H}{\Omega}\cos\beta_w + \frac{q_H}{\Omega}\sin\beta_w\right)\Big] + (A_{1c} - K_1 a_1)\left[\left(\frac{1}{8} - \frac{\varepsilon}{6}\right)\left(\frac{\dot{a}_1}{\Omega} + b_1\right)\right.$$

$$\left. - \frac{\mu}{6}a_0 + \frac{b_1}{16}(1-\varepsilon^2)\mu^2 + \frac{1}{8}\left(-\frac{p_H}{\Omega}\sin\beta_w + \frac{q_H}{\Omega}\cos\beta_w\right)\right]$$

$$+ (B_{1c} - K_1 b_1)\left[\left(\frac{1}{8} - \frac{\varepsilon}{6}\right)\left(\frac{\dot{b}_1}{\Omega} - a_1\right) + \left(\frac{\varepsilon}{4} - \frac{1}{6}\right)\mu\frac{\dot{a}_0}{\Omega} + \frac{1}{2}(1-\varepsilon^2)\left(\frac{\mu\lambda}{2} + \frac{a_1}{8}\mu^2\right)\right.$$

$$\left. + \frac{1}{8}\left(\frac{p_H}{\Omega}\cos\beta_w + \frac{q_H}{\Omega}\sin\beta_w\right)\right] - \theta_t\left[\frac{\lambda}{4} + \left(\frac{\varepsilon}{4} - \frac{1}{5}\right)\frac{\dot{a}_0}{\Omega} + \frac{\mu}{8}\left(\frac{\dot{b}_1}{\Omega}\right) - \frac{\varepsilon\mu}{6}\left(\frac{\dot{b}_1}{\Omega} - a_1\right)\right]$$

$$- \frac{1}{2}(1-\varepsilon^2)\left\{\lambda^2 + \lambda\mu a_1 + 2\lambda\varepsilon\frac{\dot{a}_0}{\Omega} + \mu\varepsilon\left[a_1\frac{\dot{a}_0}{\Omega} + a_0\left(\frac{\dot{a}_1}{\Omega} + b_1\right)\right]\right.$$

$$\left. + \mu^2\left(\frac{a_0^2}{2} + \frac{3}{8}a_1^2 + \frac{1}{8}b_1^2\right)\right\} + \frac{\mu}{3}\left[a_1\left(\frac{\dot{a}_0}{\Omega}\right) + a_0\left(\frac{\dot{a}_1}{\Omega} + b_1\right)\right] + \frac{2}{3}\lambda\left(\frac{\dot{a}_0}{\Omega}\right)$$

$$-\left[-\frac{\mu}{3}a_0 + \left(\frac{1}{4} - \frac{\varepsilon}{3}\right)\left(\frac{\dot{a}_1}{\Omega} + b_1\right)\right]\left(-\frac{p_H}{\Omega}\sin\beta_w + \frac{q_H}{\Omega}\cos\beta_w\right)$$

$$- \left(\frac{1}{4} - \frac{\varepsilon}{3}\right)\left(\frac{\dot{b}_1}{\Omega} - a_1\right)\left(\frac{p_H}{\Omega}\cos\beta_w + \frac{q_H}{\Omega}\sin\beta_w\right) - \frac{1}{8}\left(-\frac{p_H}{\Omega}\sin\beta_w + \frac{q_H}{\Omega}\cos\beta_w\right)^2$$

$$- \frac{1}{8}\left(\frac{p_H}{\Omega}\cos\beta_w + \frac{q_H}{\Omega}\sin\beta_w\right)^2 - \left(\frac{1}{4} - \frac{2}{3}\varepsilon + \frac{\varepsilon^2}{2}\right)\left\{\left(\frac{\dot{a}_0}{\Omega}\right)^2\right.$$

$$\left.\left. + \frac{1}{2}\left[\left(\frac{\dot{a}_1}{\Omega} + b_1\right)^2 + \left(\frac{\dot{b}_1}{\Omega} - a_1\right)^2\right]\right\}\right)$$

For the case of a two-bladed teetering rotor, the forces and moments can be obtained by setting $\varepsilon = 0$, $\dot{a}_0 = \ddot{a}_0 = 0$ in the above equations.

The rotor profile drag coefficient δ is required in the computation of H_W and Q. An expression for this coefficient was employed which provides a reasonable match with measured section characteristics as follows:

$$\delta = 0.009 + 0.3\left(\frac{6C_T}{a\sigma}\right)^2$$

where $(6C_T/a\sigma)$ is approximately equal to an averaged equivalent rotor blade angle of attack.

The rotor inflow ratio, defined as

$$\lambda = \frac{w_H}{\Omega R} - \frac{C_T}{2(\mu^2 + \lambda^2)^{1/2}}$$

is required in the computation of thrust. This implicit relationship is solved in the computer program through a Newton-Ralphson iterative technique.

The main rotor-induced velocity at the disk is required in subsequent calculations of the rotor-induced velocities on the helicopter components. The expression for this velocity is as follows:

$$v_i = \left(\frac{w_H}{\Omega R} - \lambda\right)\Omega R$$

Transformation T_1

The calculation of the rotor flapping dynamics and the rotor forces and moments requires the angular velocities and accelerations expressed in the hub-body system of axes and the angle of sideslip at the hub. In addition, the cyclic pitch must be expressed in the hub-wind system. The required velocities and accelerations are obtained from those expressed in the body-c.g. system as follows:

$$p_H = p \cos i_s + r \sin i_s$$

$$q_H = q$$

$$\dot{p}_H = \dot{p} \cos i_s + \dot{r} \sin i_s$$

$$\dot{q}_H = \dot{q}$$

$$u_H = [u_B - r_B(BL_{c.g.}) - q_B(WL_H - WL_{c.g.})]\cos i_s + [w_B + p_B(BL_{c.g.}) - q_B(STA_{c.g.} - STA_H)]\sin i_s$$

$$v_H = v_B + p_B(WL_H - WL_{c.g.}) + r_B(STA_{c.g.} - STA_H)$$

$$w_H = [w_B + p_B(BL_{c.g.}) - q_B(STA_{c.g.} - STA_H)]\cos i_s + [-u_B + r_B(BL_{c.g.}) + q_B(WL_H - WL_{c.g.})]\sin i_s$$

where i_s is the forward tilt of the shaft axis relative to the body-c.g. Z-axis (see fig. B-2) and STA, WL, and BL are coordinates in the aircraft reference system of axes. It is assumed that the rotor hub lies in the BL = 0 plane.

The sideslip of the rotor is then defined as:

$$\beta_w = \sin^{-1} \frac{v_H}{(v_H^2 + u_H^2)^{1/2}}$$

(β_w is defined as zero if $v_H = u_H = 0$.) Finally the cyclic pitch must be expressed in the hub-wind axis system. The expressions are:

$$A_{1c} = A_{1s} \cos \beta_w - B_{1s} \sin \beta_w$$

$$B_{1c} = A_{1s} \sin \beta_w + B_{1s} \cos \beta_w$$

Transformation T_2

The rotor forces and moments calculated in the hub-wind axes system must be expressed in the body-c.g. system as inputs to the six-degree-of-freedom rigid-body equations of motion. To accomplish this, the forces and moments are first expressed in the hub-body system of axes and then tranferred to the body-c.g. system.

The forces and moments in the x-y plane are modified by the first transformation as follows:

$$H_H = H_w \cos \beta_w + Y_w \sin \beta_w$$

$$Y_H = -H_w \sin \beta_w + Y_w \cos \beta_w$$

$$M_H = M_w \cos \beta_w + L_w \sin \beta_w$$

$$L_H = -M_w \sin \beta_w + L_w \cos \beta_w$$

The transformation to the body-c.g. system accounts for the shaft-tilt and the moment about the c.g. caused by the rotor forces. The forces expressed in the body-c.g. system are:

$$X_{MR} = T \sin i_s - H_H \cos i_s$$

$$Y_{MR} = Y_H$$

$$Z_{MR} = -T \cos i_s - H_H \sin i_s$$

The moments in the body-c.g. system are:

$$L_{MR} = L_H \cos i_s - Q \sin i_s + Y_{MR}(WL_H - WL_{c.g.}) - Z_{MR}(BL_{c.g.})$$

$$M_{MR} = M_H - Z_{MR}(STA_{c.g.} - STA_H) - X_{MR}(WL_H - WL_{c.g.})$$

$$N_{MR} = Q \cos i_s + L_H \sin i_s + X_{MR}(BL_{c.g.}) + Y_{MR}(STA_{c.g.} - STA_H)$$

APPENDIX D

TAIL ROTOR FLAPPING AND FORCE CALCULATION

The tail rotor is assumed to be teetering with a constant built-in coning a_0. The angular rate of the tail rotor is sufficiently high so that the tip-path dynamics may be ignored. Under these conditions, a_1 and b_1 in the flapping equations are assumed to be constant, and a steady-state solution of the equations is obtained to yield these quantities as follows:

$$a_{1_{TR}} = \frac{1}{\Delta_{TR}} \left[K_{1_{TR}} \left(1 + \frac{3}{2} \mu_{TR}^2\right) f_{1_{TR}} - \left(1 + \frac{\mu_{TR}^2}{2}\right) f_{2_{TR}} \right]$$

$$b_{1_{TR}} = \frac{1}{\Delta_{TR}} \left[\left(1 - \frac{\mu_{TR}^2}{2}\right) f_{1_{TR}} + K_{1_{TR}} \left(1 + \frac{\mu_{TR}^2}{2}\right) f_{2_{TR}} \right]$$

where

$$\Delta_{TR} = 1 - \frac{\mu_{TR}^4}{4} + K_{1_{TR}}^2 \left(1 + \frac{\mu_{TR}^2}{2}\right)\left(1 + \frac{3}{2} \mu_{TR}^2\right)$$

$$f_{1_{TR}} = \frac{4}{3} \mu_{TR} a_{0_{TR}} - \frac{16}{\gamma_{TR} \Omega_{TR}} p_{TR} - \frac{q_{TR}}{\Omega_{TR}}$$

$$f_{2_{TR}} = \frac{8}{3} K_{1_{TR}} \mu_{TR} a_{0_{TR}} + \frac{16\ q_{TR}}{\gamma_{TR} \Omega_{TR}} - \mu_{TR} \left(\frac{8}{3} \theta_{0_{TR}} + 2\theta_{t_{TR}} + 2\lambda_{TR} - \frac{p_{TR}}{\Omega_{TR}}\right.$$

The forces on the tail rotor are then calculated as follows:

$$T_{TR} = \rho a_{TR} c_{TR} R_{TR} (\Omega_{TR} R_{TR})^2 \left[\frac{\lambda_{TR}}{2} + \theta_{0_{TR}} \left(\frac{1}{3} + \frac{\mu_{TR}^2}{2}\right) + \frac{\theta_{t_{TR}}}{4} (1 + \mu_{TR}^2) + \frac{\mu_{TR} K_{1_{TR}}}{2} b_{1_{TR}} \right.$$

$$\left. - a_{0_{TR}} \left(\frac{1}{3} + \frac{\mu_{TR}^2}{2}\right) K_{1_{TR}} + \frac{\mu_{TR}}{4} \frac{p_{TR}}{\Omega_{TR}} \right]$$

$$Q_{TR} = \rho a_{TR} c_{TR} R_{TR}^2 (\Omega_{TR} R_{TR})^2 \left\{ \frac{\delta_{TR}}{4a_{TR}} (1 + \mu_{TR}^2) - \frac{\lambda_{TR}}{3} (\theta_{0_{TR}} - K_{1_{TR}} a_{0_{TR}}) - \frac{\theta_{t_{TR}} \lambda_{TR}}{4} \right.$$

$$- K_{1_{TR}} \left[a_{1_{TR}} \left(\frac{b_{1_{TR}}}{8} - \frac{\mu_{TR}}{6} a_{0_{TR}} + \frac{b_{1_{TR}} \mu_{TR}^2}{16} \right) + b_{1_{TR}} \left(- \frac{a_{1_{TR}}}{8} + \frac{\mu_{TR} \lambda_{TR}}{4} + \frac{a_{1_{TR}} \mu_{TR}^2}{16} \right) \right]$$

$$- \frac{1}{2} \left[\lambda_{TR}^2 + \lambda_{TR} \mu_{TR} a_{1_{TR}} + \mu_{TR}^2 \left(\frac{a_{0_{TR}}^2}{2} + \frac{3}{8} a_{1_{TR}}^2 + \frac{b_{1_{TR}}^2}{8} \right) \right]$$

$$+ \frac{\mu_{TR}}{3} a_{0_{TR}} b_{1_{TR}} - \frac{1}{8} (a_{1_{TR}}^2 + b_{1_{TR}}^2) - \left[\frac{\mu_{TR}}{6} (\theta_{0_{TR}} - K_{1_{TR}} a_{0_{TR}}) \right.$$

$$\left. + \frac{1}{8} K_{1_{TR}} b_{1_{TR}} - \frac{a_{1_{TR}}}{4} \right] \frac{p_{TR}}{\Omega_{TR}} - \left(\frac{1}{8} K_{1_{TR}} a_{1_{TR}} + \frac{b_{1_{TR}}}{4} - \frac{\mu_{TR} a_{0_{TR}}}{3} \right) \frac{q_{TR}}{\Omega_{TR}}$$

$$\left. - \frac{1}{8} \left[\left(\frac{p_{TR}}{\Omega_{TR}} \right)^2 + \left(\frac{q_{TR}}{\Omega_{TR}} \right)^2 \right] \right\}$$

The positive directions for tail rotor torque and rotation are shown on figure D-1.

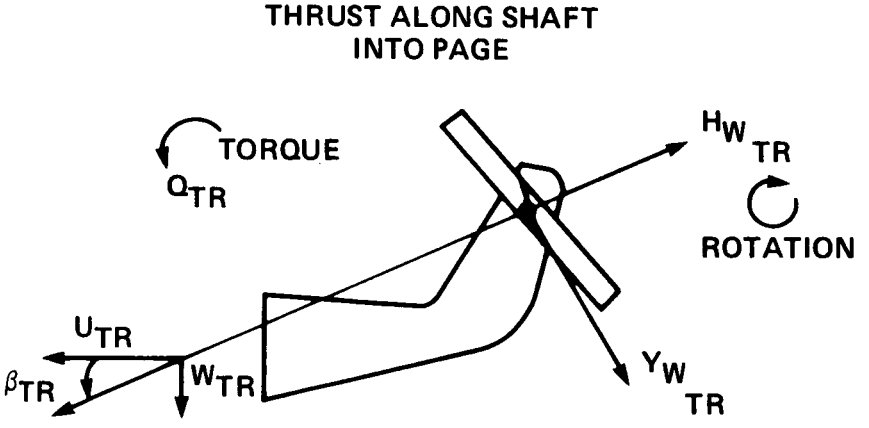

Figure D-1.- Tail rotor forces and moments.

$$H_{W_{TR}} = \rho a_{TR} c_{TR} R_{TR} (\Omega_{TR} R_{TR})^2 \left\{ \frac{\delta_{TR} \mu_{TR}}{2a_{TR}} - \frac{1}{4} (\theta_{0_{TR}} - K_{1_{TR}} a_{0_{TR}}) \left(2\lambda_{TR} \mu_{TR} - \frac{4}{3} a_{1_{TR}} \right) \right.$$

$$- \frac{\theta_{t_{TR}}}{4} (\mu_{TR} \lambda_{TR} - a_{1_{TR}}) - \frac{1}{4} K_{1_{TR}} \left[\frac{2}{3} a_{0_{TR}} a_{1_{TR}} + b_{1_{TR}} (\lambda_{TR} - a_{1_{TR}} \mu_{TR}) \right]$$

$$+ \frac{3}{4} \lambda_{TR} a_{1_{TR}} - \frac{a_{0_{TR}} b_{1_{TR}}}{6} + \frac{\mu_{TR}}{4} (a_{0_{TR}}^2 + a_{1_{TR}}^2)$$

$$\left. - \frac{1}{6} (\theta_{0_{TR}} - K_{1_{TR}} a_{0_{TR}}) + \frac{\theta_{t_{TR}}}{8} + \frac{3}{16} K_{1_{TR}} b_{1_{TR}} \mu_{TR} + \frac{\lambda_{TR}}{2} + \frac{a_{1_{TR}} \mu_{1_{TR}}}{16} \right] \frac{p_{TR}}{\Omega_{TR}}$$

$$\left. - \left(\frac{1}{16} K_{1_{TR}} a_{1_{TR}} \mu_{TR} + \frac{a_{0_{TR}}}{6} + \frac{b_{1_{TR}} \mu_{TR}}{16} \right) \frac{q_{TR}}{\Omega_{TR}} \right\}$$

$$Y_{W_{TR}} = \rho a_{TR} c_{TR} R_{TR} (\Omega_{TR} R_{TR})^2 \left\{ - \frac{1}{4} (\theta_{0_{TR}} - K_{1_{TR}} a_{0_{TR}}) \left(- \frac{4}{3} b_{1_{TR}} + 3a_{0_{TR}} \mu_{TR} - 2b_{1_{TR}} \mu_{TR}^2 \right) \right.$$

$$- \frac{\theta_{t_{TR}}}{4} (-b_{1_{TR}} + 2a_{0_{TR}} \mu_{TR} - b_{1_{TR}} \mu_{TR}^2) + \frac{K_{1_{TR}}}{4} \left[a_{1_{TR}} (\lambda_{TR} + a_{1_{TR}} \mu_{TR}) \right.$$

$$\left. \left. + b_{1_{TR}} \left(- \frac{2}{3} a_{0_{TR}} + 2b_{1_{TR}} \mu_{TR} - 2a_{0_{TR}} \mu_{TR}^2 \right) \right] + \frac{3}{4} b_{1_{TR}} \lambda_{TR} + \frac{1}{6} a_{0_{TR}} a_{1_{TR}} \right.$$

$$- \frac{\mu_{TR}}{4} (6a_{0_{TR}} \lambda_{TR} - a_{1_{TR}} b_{1_{TR}}) - \mu_{TR}^2 a_{0_{TR}} a_{1_{TR}} + \left(\frac{1}{16} K_{1_{TR}} a_{1_{TR}} \mu_{TR} - \frac{a_{0_{TR}}}{6} \right.$$

$$\left. + \frac{5}{16} b_{1_{TR}} \mu_{TR} \right) \frac{p_{TR}}{\Omega_{TR}} + \left[\frac{1}{6} (\theta_{0_{TR}} - K_{1_{TR}} a_{0_{TR}}) + \frac{\theta_{t_{TR}}}{8} + \frac{1}{16} K_{1_{TR}} b_{1_{TR}} \mu_{TR} \right.$$

$$\left. \left. + \frac{1}{2} \lambda_{TR} + \frac{7}{16} a_{1_{TR}} \mu_{TR} \right] \frac{q_{TR}}{\Omega_{TR}} \right\}$$

The rotor blade profile drag coefficient, δ, is required in the computation of H_{TR} and Q_{TR}. This is calculated similarly to the case of the main rotor as follows:

$$\delta_{TR} = 0.009 + 0.3 \left(\frac{6C_{T_{TR}}}{\sigma_{TR} a_{TR}} \right)^2$$

The inflow ratio, as in the case of the main rotor, must be calculated from the following relationship:

$$\lambda_{TR} = \frac{-v_{TR}}{\Omega_{TR} R_{TR}} - \frac{C_{T_{TR}}}{2\sqrt{\mu_{TR}^2 + \lambda_{TR}^2}}$$

This implicit relationship is solved through an iteration procedure.

Main Rotor Interference and Transformation T_3

The calculation of the tail rotor forces and moments requires the local flow velocity components in the hub-wind axes system for the tail rotor. The velocity at the tail rotor includes provision for the downwash contributed by the flow field of the main rotor. For these calculations, the tail rotor is assumed to lie in the x-z plane.

The velocities at the rotor hub in an axis system co-directional with the body-c.g. system are:

$$u_{TR} = u_B$$

$$v_{TR} = v_B + p_B(WL_{TR} - WL_{c.g.}) - r_B(STA_{TR} - STA_{c.g.})$$

$$w_{TR} = w_B + q_B(STA_{TR} - STA_{c.g.}) + w_{i_{TR}}$$

The quantity $w_{i_{TR}}$ is the downwash velocity due to the main rotor. The downwash velocity is represented in the modes as a function of the wake angle χ and sideslip. The variation of the downwash varies nonlinearly with location in the wake. Therefore, the downwash must be determined uniquely for each location from data such as those published in reference 10. The representation in the model consists of the downwash expressed as a function of a power series in the wake angle at angles of sideslip of 0°, ±90°, and 180° as follows:

$$\left(\frac{w_{i_{TR}}}{v_i}\right) = \sum_{n=0}^{4} k_n \chi^n$$

where v_i is the momentum-theory value of the rotor-induced velocity. The coordinate system employed in reference 10 is centered at the hub, and the X and Y axes lie in the tip-path plane. Accordingly, the tail rotor location in this coordinate system varies with the value of a_1, the tilt of the tip-path plane. In view of the approximate nature of the wake estimate, which can vary widely with disk load distribution, inclusion of this level of detail is unwarranted. Accordingly, the downwash is estimated for a constant location referenced to the hub-body system and the wake angle referred to that system. Hence,

$$\chi = \tan^{-1}\left(\frac{\mu}{\lambda}\right)$$

Interpolation for the value of the downwash at arbitrary sideslip angles is accomplished as in the following example, where β has been determined to be between ±90°:

$$w_{i_{TR}} = \left[\left(\frac{w_{i_{TR}}}{v_i}\right)_{\beta=0} |\cos\beta| + \left(\frac{w_{i_{TR}}}{v_i}\right)_{\beta=90} |\sin\beta|\right] v_i$$

Similarly, when $90° < \beta < 270°$, the downwash is calculated as follows:

$$w_{i_{TR}} = \left[\left(\frac{w_{i_{TR}}}{v_i}\right)_{\beta=180} |\cos \beta| + \left(\frac{w_{i_{TR}}}{v_i}\right)_{\beta=90} |\sin \beta|\right] v_i$$

The advance ratio for the tail rotor, which is assumed to be in the x-z plane, is then:

$$\mu_{TR} = \frac{\sqrt{u_{TR}^2 + w_{TR}^2}}{\Omega_{TR} R_{TR}}$$

and the rotor sideslip angle is defined for the tail rotor as:

$$\beta_{TR} = \tan^{-1}\left(\frac{w_{TR}}{u_{TR}}\right)$$

Then, in the hub-wind axis system defined for the tail rotor, the angular velocities are:

$$p_{TR} = p_B \cos \beta_{TR} + r_B \sin \beta_{TR}$$

$$q_{TR} = r_B \cos \beta_{TR} - p_B \sin \beta_{TR}$$

Transformation T_4

The transformation to express the tail rotor forces and moments in the body-c.g. system of axes is as follows:

$$X_{TR} = -(Y_{TR})_W \sin \beta_{TR} - (H_{TR})_W \cos \beta_{TR}$$

$$Y_{TR} = T_{TR}$$

$$Z_{TR} = (Y_{TR})\cos \beta_{TR} - (H_{TR})_W \sin \beta_{TR}$$

$$L_{TR} = Y_{TR}(WL_{TR} - WL_{c.g.})$$

$$M_{TR} = -Q_{TR} + Z_{TR}(STA_{TR} - STA_{c.g.}) - X_{TR}(WL_{TR} - WL_{c.g.})$$

$$N_{TR} = -Y_{TR}(STA_{TR} - STA_{c.g.})$$

APPENDIX E

EMPENNAGE FORCES AND MOMENTS

The expressions for the lift and drag coefficients for the vertical fin and the horizontal stabilizer are identical when referenced to a local wind-axes system for the particular surface. (See appendix B.)

The conditions at the stall of each surface are defined as follows:

$$\alpha_s = \frac{C_{L_M}}{a} \qquad \alpha_s \leq \frac{\pi}{4}$$

$$\alpha_s = \frac{\pi}{4} \qquad \alpha_s > \frac{\pi}{4}$$

$$\alpha_1 = 1.2\alpha_s$$

$$C_{L_M} = C_{L_M} \qquad \alpha_s \leq \frac{\pi}{4}$$

$$C_{L_M} = a\,\frac{\pi}{4} \qquad \alpha_s > \frac{\pi}{4}$$

The angle of attack for input into the expressions for the lift and drag coefficient is:

$$\alpha_i = \alpha \qquad 0 \leq \alpha < \frac{\pi}{2}$$

$$\alpha_i = -\alpha \qquad -\frac{\pi}{2} \leq \alpha < 0$$

$$\alpha_i = \pi - \alpha \qquad \frac{\pi}{2} \leq \alpha < \pi$$

$$\alpha_i = \pi + \alpha \qquad -\pi \leq \alpha < -\frac{\pi}{2}$$

where α_i represents the angle-of-attack input to the lift and drag equations.

The lift and drag coefficients are calculated using the following expressions:

$$C_{L_0} = a\alpha_i \qquad 0 \leq \alpha_i < \alpha_s$$

$$C_{L_0} = C_{L_M} - a(\alpha_i - \alpha_s) \qquad \alpha_s < \alpha_i < \alpha_1$$

$$C_{L_0} = 0.8C_{L_M}\left[1 - \left(\frac{\alpha_i - \alpha_1}{\pi/2 - \alpha_1}\right)^2\right] \qquad \alpha_1 \leq \alpha_i \leq \frac{\pi}{2}$$

$$C_{D_P} = 0.009 + 0.11\alpha_i^2 \qquad 0 \leq \alpha_i \leq 0.35$$

$$C_{D_P} = -0.1254 + 0.9415\alpha_i + 0.977525 \sin^2\alpha_i \qquad 0.35 < \alpha_i < \frac{\pi}{2}$$

where C_{D_P} is the profile drag coefficient.

$$C_D = C_{D_P} + \frac{C_L^2}{0.8\pi AR}$$

Depending on the quadrant in which the angle of attack lies, the lift coefficient for the surface is:

$$C_L = C_{L_0} \qquad 0 \leq \alpha < \frac{\pi}{2}$$

$$C_L = -C_{L_0} \qquad -\frac{\pi}{2} \leq \alpha < \pi$$

$$C_L = -0.8C_{L_0} \qquad \frac{\pi}{2} \leq \alpha < \pi$$

$$C_L = 0.8C_{L_0} \qquad -\pi \leq \alpha < -\frac{\pi}{2}$$

Horizontal Tail

The lift curve slope of the horizontal tail is calculated from elementary lifting line theory and is corrected for sideslip as follows:

$$\alpha_{HS} = \left(\frac{2\pi}{1 + 2/AR_{HS}}\right) \cos^2\beta_{HS}$$

Main rotor interference and transformation T_5- The velocity at the horizontal tail includes a factor to account for rotor downwash, $w_{i_{HT}}$. This factor is calculated similarly to that calculated for the tail rotor. In calculating the velocities at the horizontal tail, the relatively small contribution of roll rate is ignored. The expressions for the velocity components at the horizontal tail are as follows:

$$u_{HS} = u_B$$

$$v_{HS} = v_B - r_B(STA_{HS} - STA_{c.g.})$$

$$w_{HS} = w_B + q_B(STA_{HS} - STA_{c.g.}) + w_{i_{HT}}$$

The angle of attack and angle of sideslip of the horizontal tail are then:

$$\alpha_{HS} = \tan^{-1}\left(\frac{w_{HS}}{u_{HS}}\right) + i_{HS}$$

$$\beta_{HS} = \sin^{-1}\left(\frac{v_{HS}}{V_{HS}}\right)$$

where

$$V_{HS} = \sqrt{u_{HS}^2 + v_{HS}^2 + w_{HS}^2}$$

The angle i_{HS} is the incidence of the horizontal tail. Note that the effect of a cambered surface may be accounted for by selecting this parameter to differ from the angle of the chord plane by an amount equal to the angle of attack for zero lift.

The factor employed to calculate lift and drag forces from the lift and drag coefficients is:

$$F_{HS} = \frac{1}{2} \rho V_{HS}^2 S_{HS} \eta_{HS}$$

where the constant η_{HS} is used to account for fuselage blockage or the horizontal tail area considered to be within the fuselage.

Transformation T_6- The forces in the body-c.g. system of axes attributed to the horizontal tail are:

$$X_{HS} = F_{HS}(-C_{D_{HS}} \cos \beta_{HS} \cos \alpha_{HS} + C_{L_{HS}} \sin \alpha_{HS})$$

$$Y_{HS} = F_{HS}(-C_{D_{HS}} \sin \beta_{HS})$$

$$Z_{HS} = F_{HS}(-C_{L_{HS}} \cos \alpha_{HS} - C_{D_{HS}} \cos \beta_{HS} \sin \alpha_{HS})$$

The forces are assumed to act at the quarter chord point of the horizontal tail at a spanwise location corresponding to the center of area. The moments are:

$$L_{HS} = Y_{HS}(WL_{HS} - WL_{c.g.}) + Z_{HS}(BL_{HS})$$

$$M_{HS} = -X_{HS}(WL_{HS} - WL_{c.g.}) + Z_{HS}(STA_{HS} - STA_{c.g.})$$

$$N_{HS} = -X_{HS}(BL_{HS}) - Y_{HS}(STA_{HS} - STA_{c.g.})$$

Vertical Fin

The estimate of the lift curve slope of the vertical fin includes the effect of sweep as well as of sideslip as follows:

$$a_F = \left(\frac{2\pi}{1 + 2/AR_F}\right) \cos^2(\beta_F + \Lambda_F)$$

Transformation T_7- The computation of the velocity at the vertical fin ignores the small contribution from roll rate and includes a term in the sidewash due to the induced velocity of the tail rotor. The three components of velocity are as follows:

$$u_F = u_B$$

$$v_F = v_B - r_B(STA_F - STA_{c.g.}) + v_{i_{TR}} k v_{TR}$$

$$w_F = w_B + q_B(STA_F - STA_{c.g.}) + w_{i_F}$$

The constant kv_{TR} can be adjusted to account for the fraction of the vertical tail immersed in the tail rotor wake. The main rotor interference factor w_{i_F} is computed similarly to the factor for downwash at the tail rotor.

The angles of attack and sideslip of the vertical fin in the local wind coordinate system are:

$$\alpha_F = \tan^{-1}\left(\frac{v_F}{u_F}\right) + i_F$$

$$\beta_F = \sin^{-1}\left(\frac{w_F}{V_F}\right)$$

where

$$V_F = \sqrt{u_F^2 + v_F^2 + w_F^2}$$

As in the case of the horizontal tail, the angle i_F can be adjusted to account for camber of the vertical fin.

APPENDIX F

CALCULATION OF FUSELAGE FORCES AND MOMENTS

In calculating the fuselage forces and moments, it is assumed that the longitudinal forces and moments are dependent on angle of attack and the lateral forces and moments are dependent on angle of sideslip. The exception is the drag force, which is assumed to have a contribution from both angle of attack and sideslip. This representation is a gross simplification, and if detailed test data are available on which to base a more sophisticated representation, they should be substituted. (See, e.g., ref. 8.)

Low-angle approximation $\alpha,\beta = -15°$ to $15°$

$$L = q_f \left(\frac{L_0}{q} + \frac{\partial L/q}{\partial \alpha}\,\alpha\right) \qquad Y = q_f \left(\frac{\partial Y/q}{\partial \beta}\,\beta\right)$$

$$D_\alpha = q_f \left(\frac{D_0}{q} + \frac{\partial D}{\partial \alpha}\,\alpha + \frac{\partial^2 D}{\partial \alpha^2}\,\alpha^2\right) \qquad \ell = q_f \left(\frac{\partial \ell/q}{\partial \beta}\,\beta\right)$$

$$M = q_f \left(\frac{M_0}{q} + \frac{\partial M/q}{\partial \alpha}\,\alpha\right) \qquad N = q_f \left(\frac{\partial N/q}{\partial \beta}\,\beta\right)$$

$$D = D_\alpha + D_\beta \qquad D_\beta = q_f \left(\frac{\partial^2 D/q}{\partial \beta^2}\,\beta^2\right)$$

High-angle approximation

$$L = q_f \left(\frac{D_{\alpha=90°}}{q_f}\,|\sin\alpha|\,\sin\alpha\cos\alpha\right) \qquad Y = q_f \left(\frac{-D_{\beta=90°}}{q_f}\,|\sin\beta|\,\sin\beta\cos\beta\right)$$

$$D_\alpha = q_f \left(\frac{D_{\alpha=90°}}{q_f}\,|\sin\alpha|\,\sin^2\alpha\right) \qquad \ell = q_f \left(\frac{\ell_{\beta=90°}}{q_f}\,|\sin\beta|\,\sin\beta\right)$$

$$M = q_f (M_{\alpha=90°}\,|\sin\alpha|\,\sin\alpha) \qquad N = q_f (N_{\beta=90°}\,|\sin\beta|\,\sin\beta)$$

$$D = D_\alpha + D_\beta \qquad D_\beta = q_f (D_{\beta=90°}\,|\sin\beta|\,\sin\beta^2)$$

Phasing between the low-angle approximation and the high-angle approximation is based on a complex phase angle and linear interpolation. The complex phase angle is given by:

$$\pi_{FUS} = \cos^{-1}\left(\frac{u_f}{V_f}\right)$$

Linear interpolation based on this phase angle is employed over the range of $15° < |\pi_{FUS}| < 30°$.

Main rotor interference and transformation T_9- The fuselage angles of attack, angle of sideslip, and dynamic pressure include an averaged effect of rotor downwash. The expression for downwash was obtained for typical single rotor helicopters from an empirical fit to data presented in reference 10. The velocities on the fuselage are as follows:

$$u_f = u_B$$

$$v_f = v_B$$

$$w_f = w_B + w_{i_f}$$

Where w_{i_f} is the induced velocity due to the rotor and is defined as:

$$w_{i_f} = \left(\frac{w_{i_f}}{v_i}\right) v_i$$

$$\left(\frac{w_{i_f}}{v_i}\right) = 1.299 + 0.671\chi - 1.172\chi^2 + 0.351\chi^3$$

The rotor wake angle χ is defined as:

$$\chi = \tan^{-1}\left(\frac{\mu}{-\lambda}\right)$$

The angles of attack and sideslip are then:

$$\alpha_f = \tan^{-1}\frac{w_f}{u_f}$$

$$\beta_f = \sin^{-1}\frac{v_f}{V_f}$$

where

$$V_f = \sqrt{u_f^2 + v_f^2 + w_f^2}$$

The dynamic pressure on the fuselage is based on the velocity, including the effect of rotor downwash.

$$q_f = \frac{1}{2}\rho V_f^2$$

Transformation T_{10}- The fuselage forces and moments are calculated in the wind system of axes about the fuselage reference point. The transformation must transfer the moment to the center of gravity and express all forces and moments in the body system of axes.

The forces and moments in the body-c.g. system of axes are given by the following equations:

$$X_f = -D \cos \beta \cos \alpha - Y \sin \beta \sin \alpha + L \sin \alpha$$

$$Y_f = Y \cos \beta - D \sin \beta$$

$$Z_f = -L \cos \alpha - D \cos \beta \sin \alpha - Y \sin \beta \sin \alpha$$

$$L_f = \ell \cos \beta \cos \alpha - M \sin \beta \cos \alpha - N \sin \alpha + Y_f(WL_{ACF} - WL_{c.g.}) - Z_{f_{BL_{c.g.}}}$$

$$M_f = M \cos \beta + \ell \sin \beta - X_f(WL_{ACF} - WL_{c.g.}) + Z_f(STA_{ACF} - STA_{c.g.})$$

$$N_f = N \cos \alpha + \ell \cos \beta \cos \alpha - M \sin \beta \sin \alpha + Y_f(STA_{c.g.} - STA_{ACF}) + X_f(BL_{c.g.})$$

RPM GOVERNOR

The rpm governor model provides for an rpm degree of freedom with simple engine and governor dynamics. When the rpm governor option is used, the main rotor and tail rotor speeds are changed based on current torque requirements and engine power available. Trim initial conditions establish baseline values of rotor speed and engine torque. Flight variations from that trim condition result in changing torque requirements which cause rotor speed variations which feed through the governor control laws to provide fuel flow changes. The fuel flow changes provide engine power changes which are converted to engine torque available.

The rpm degree of freedom may be described by the equation:

$$Q_E - Q_R = J\dot{\Omega}$$

where:

Q_E = engine torque

Q_R = required rotor torque

J = rotor rotational inertia

$\dot{\Omega}$ = rotor speed rate of change

For low flapping hinge offsets, the rotational inertia, J, may be approximated from the blade flapping inertia, I_β:

$$J = NI_\beta$$

where N is the number of blades.

The main rotor torque required is a complicated function of many variables including blade pitch settings, airspeed, inflow velocity, flapping angles, and rotor speed. The torque equation provides the necessary calculation. The rotor speed governing of this model uses linear control theory based on an operating point. Thus, the rotor speed, Ω, takes the form:

$$\Omega = \Omega_0 + \Delta\Omega$$

where Ω_0 is the trim rotor speed and $\Delta\Omega$ is the rotor-speed variation.

A detailed representation of engine torque requires a complicated nonlinear function of many variables including operating power setting, ambient pressure and temperature, and fuel flow, w_f. For this simplified model, rpm governing acts on fuel flow to control engine torque. A gas turbine engine produces power which must be converted to torque based on the current rotor speed.

$$Q_E = \frac{550}{\Omega} HP$$

It is important to note that the current rotor speed is used, not the operating point speed, Ω_0. Thus, the power-to-torque conversion factor is always changing.

The engine power response to fuel flow is simply modeled as a first order lag:

$$\Delta HP = \frac{K_E}{1 + \tau_E s} \Delta w_f$$

The time constant, τ_E, and gain, K_E, are selected based on engine characteristics and operating point.

The complete rpm degree of freedom and engine-governor model is shown in figure 3.

Note that a throttle on/off switch has been added to allow turning the power on or off. A separate time constant for the throttle is provided to allow for a large power change time constant for the throttle and a small power change time constant for normal engine operation.

The governor control law is given by:

$$\Delta w_f = -\left(Kg_1 + \frac{Kg_2}{s} + Kg_3 s\right)\Delta\Omega$$

which provides proportional, integral, and rate feedback.

APPENDIX H

COCKPIT CONTROLS AND CYCLIC CONTROL PHASING

Cyclic, collective, and pedal controls may be specified from a zero position either centered or full left or down. The cyclic control position must be consistent between longitudinal and lateral cyclic, that is, centered or full left and forward. The zero position of the collective or pedals may be specified independently. The table below lists the zero position, positive direction, and sign of the moment or force produced in the body system of axes. Alternate control zero position conventions are listed in parentheses.

Control	Zero position	Positive direction	Moment/force
Longitudinal cyclic, δ_e	Centered (full forward)	Aft	+M
Lateral cyclic, δ_a	Centered (full left)	Right	+L
Collective, δ_c	Full down	Up	-Z
Pedals, δ_p	Centered (full left)	Right pedal forward	+N

The control gearing, rigging, and cyclic control phasing are governed by the following equations:

$$A_{1_S} = C_1\delta_a + C_3\delta_e + C_{A_{1_S}}$$

$$B_{1_S} = C_2\delta_a + C_4\delta_e + C_{B_{1_S}}$$

$$\theta_0 = C_6\delta_c + C_5$$

$$\theta_{0_{TR}} = C_8\delta_p + C_7$$

The terms $C_{A_{1_S}}$, $C_{B_{1_S}}$, C_5, and C_7 are the constant or rigging terms for each control. The terms C_1 through C_4 can be used to adjust for the phase angle between the cyclic control input and the resulting flapping. These phase angle terms may be specified in two ways. First, a cyclic control phase relationship may be specified on the basis of main rotor dynamic properties:

$$PP = \frac{K_\beta}{I_\beta\Omega^2} + \frac{\varepsilon RM_\beta}{gI_\beta} + \frac{\gamma k_1}{8}\left(1 - \frac{4}{3}\varepsilon\right)$$

$$C_1 = \frac{1 - (8/3)\varepsilon + 2\varepsilon^2}{1 - (4/3)\varepsilon} \quad (CK2)$$

$$C_2 = \frac{8(PP)(CK2)}{\gamma[1 - (4/3)\varepsilon]}$$

$$C_3 = C_2\left(\frac{CK1}{CK2}\right)$$

$$C_4 = -C_1\left(\frac{CK1}{CK2}\right)$$

The terms CK1 and CK2 are the longitudinal and lateral cyclic control sensitivities, respectively. As an alternative, a control phase angle, ψ_0, may be specified, which provides the following relationships:

$$C_1 = (CK2)\cos\psi_0$$

$$C_2 = (CK2)\sin\psi_0$$

$$C_3 = C_2\left(\frac{CK1}{CK2}\right)$$

$$C_4 = -C_1\left(\frac{CK1}{CK2}\right)$$

APPENDIX I

LINEARIZED SIX-DEGREE-OF-FREEDOM REPRESENTATION OF HELICOPTER DYNAMICS

The linear, first-order set of differential equations describing the rigid body motion of the helicopter are of the form:

$$\dot{x} = [F]x + [G]\delta$$

where x represents the perturbations from trim of the state variables u_B, w_B, q_B, Θ, v_B, p_B, ϕ, and r_B; and δ represents the deviations from the trim control positions of δ_e, δ_c, δ_a, and δ_p. The linear representation is valid only if the initial angular velocities p_B, q_B, and r_B are zero.

The elements of the F and G matrices are of two types. The first type consists of inertial and gravitational terms that can be obtained analytically from the equations of motion. The second type consists of partial derivatives arising from aerodynamic forces and moments. The force and moment derivatives are obtained by considering both position and negative perturbations from trim. For example:

$$X_u = \frac{\partial X}{\partial u} \cong \frac{X(u_0 + \Delta u) - X(u_0 - \Delta u)}{2\ \Delta u}$$

The elements of the F and G matrices and the state variable vectors are given in table I-1.

TABLE I-1.- ELEMENTS OF THE LINEARIZED EQUATIONS OF MOTION

$X = (\Delta u_B,\ \Delta w_B,\ \Delta q_B,\ \Delta\Theta,\ \Delta v_B,\ \Delta p_B,\ \Delta\phi,\ \Delta r_B)^T$

$\delta = (\Delta\delta_e,\ \Delta\delta_c,\ \Delta\delta_a,\ \Delta\delta_p)^T$

$$F = \begin{bmatrix}
\frac{X_u}{m} & \frac{X_w}{m} & \frac{X_q}{m} - w_0 & -g\cos\Theta_0 & \frac{X_v}{m} & \frac{X_p}{m} & 0 & \frac{X_r}{m} + v_0 \\
\frac{Z_u}{m} & \frac{Z_w}{m} & \frac{Z_q}{m} + u_0 & -g\cos\phi_0\sin\Theta_0 & \frac{Z_v}{m} & \frac{Z_p}{m} - v_0 & -g\sin\phi_0\cos\Theta_0 & \frac{Z_r}{m} \\
\frac{M_u}{I_y} & \frac{M_w}{I_y} & \frac{M_q}{I_y} & 0 & \frac{M_v}{I_y} & \frac{M_p}{I_y} & 0 & \frac{M_r}{I_y} \\
0 & 0 & \cos\phi_0 & 0 & 0 & 0 & 0 & -\sin\phi_0 \\
\frac{Y_u}{m} & \frac{Y_w}{m} & \frac{Y_q}{m} & -g\sin\phi_0\sin\Theta_0 & \frac{Y_v}{m} & \frac{Y_p}{m} + w_0 & g\cos\phi_0\cos\Theta_0 & \frac{Y_r}{m} - u_0 \\
\frac{(I_zL_u + I_{xz}N_u)}{I_c} & \frac{(I_zL_w + I_{xz}N_w)}{I_c} & \frac{(I_zL_q + I_{xz}N_q)}{I_c} & 0 & \frac{(I_zL_v + I_{xz}N_v)}{I_c} & \frac{(I_zL_p + I_{xz}N_p)}{I_c} & 0 & \frac{(I_zL_r + I_{xz}N_r)}{I_c} \\
0 & 0 & \sin\phi_0\tan\Theta_0 & 0 & 0 & 1 & 0 & \cos\phi_0\tan\Theta_0 \\
\frac{(I_{xz}L_u + I_xN_u)}{I_c} & \frac{(I_{xz}L_w + I_xN_w)}{I_c} & \frac{(I_{xz}L_q + I_xN_q)}{I_c} & 0 & \frac{(I_{xz}L_v + I_xN_v)}{I_c} & \frac{(I_{xz}L_p + I_xN_p)}{I_c} & 0 & \frac{(I_{xz}L_r + I_xN_r)}{I_c}
\end{bmatrix}$$

$I_c = (I_xI_z - I_{xz}^2)$

$$G = \begin{bmatrix}
\frac{X_{\delta_e}}{m} & \frac{X_{\delta_c}}{m} & \frac{X_{\delta_a}}{m} & \frac{X_{\delta_p}}{m} \\
\frac{Z_{\delta_e}}{m} & \frac{Z_{\delta_c}}{m} & \frac{Z_{\delta_a}}{m} & \frac{Z_{\delta_p}}{m} \\
\frac{M_{\delta_e}}{I_y} & \frac{M_{\delta_c}}{I_y} & \frac{M_{\delta_a}}{I_y} & \frac{M_{\delta_p}}{I_y} \\
0 & 0 & 0 & 0 \\
\frac{Y_{\delta_e}}{m} & \frac{Y_{\delta_c}}{m} & \frac{Y_{\delta_a}}{m} & \frac{Y_{\delta_p}}{m} \\
\frac{(I_zL_{\delta_e} + I_{xz}N_{\delta_e})}{I_c} & \frac{(I_zL_{\delta_c} + I_{xz}N_{\delta_c})}{I_c} & \frac{(I_zL_{\delta_a} + I_{xz}N_{\delta_a})}{I_c} & \frac{(I_zL_{\delta_p} + I_{xz}N_{\delta_p})}{I_c} \\
0 & 0 & 0 & 0 \\
\frac{(I_{xz}L_{\delta_e} + I_xN_{\delta_e})}{I_c} & \frac{(I_{xz}L_{\delta_c} + I_xN_{\delta_c})}{I_c} & \frac{(I_{xz}L_{\delta_a} + I_xN_{\delta_a})}{I_c} & \frac{(I_{xz}L_{\delta_p} + I_xN_{\delta_p})}{I_c}
\end{bmatrix}$$

APPENDIX J

CONFIGURATION DESCRIPTION REQUIREMENTS

Table J-1 lists the parameters required to describe a helicopter configuration for use in the computer simulation. Listed are the parameter name, algebraic symbol, computer mnemonic, and units for each parameter. In addition, an example value based on an AH-1G is provided for each parameter. AH-1G parameters are based on values in reference 8.

TABLE J-1.- CONFIGURATION DESCRIPTION REQUIREMENTS

Name	Algebraic symbol	Computer mnemonic	Units	Example value
Main rotor (MR) group				
MR rotor radius	R_{MR}	ROTOR	ft	22
MR chord	c_{MR}	CHORD	ft	2.25
MR rotational speed	Ω_{MR}	OMEGA	rad/sec	32.88
Number of blades	n_b	BLADES	N-D	2
MR Lock number	γ_{MR}	GAMMA	N-D	5.216
MR hinge offset	ϵ	EPSLN	percent/100	0
MR flapping spring constant	K_β	AKBETA	lb-ft/rad	0
MR pitch-flap coupling tangent of δ_3	K_1	AKONE	N-D	0
MR blade twist	$\Theta_{t_{MR}}$	THETT	rad	-0.17453
MR precone angle (required for teetering rotor)	$a_{0_{MR}}$	AOP	rad	0.048
MR solidity	σ_{MR}	SIGMA	N-D	0.0651
MR lift curve slope	a_{MR}	ASLOPE	rad^{-1}	6.28
MR maximum thrust	$C_{T_{max}}$	CTM	N-D	0.165
MR longitudinal shaft tilt (positive forward)	i_s	CIS	rad	0
MR hub stationline	STA_H	STAH	in.	200
MR hub waterline	WL_H	WLH	in.	152.76
Tail rotor (TR) group				
TR radius	R_{TR}	RTR	ft	4.25
TR rotational speed	Ω_{TR}	OMTR	rad/sec	168.44
TR Lock number	γ_{TR}	GAMATR	N-D	2.2337
TR solidity	σ_{TR}	STR	N-D	0.105
TR pitch-flap coupling tangent of δ_3	$K_{1_{TR}}$	FKITR	N-D	0.5773
TR precone	$a_{0_{TR}}$	AOTR	rad	0.02618
TR blade twist	$\Theta_{t_{TR}}$	THETR	rad	0
TR lift curve slope	a_{TR}	ATR	rad^{-1}	6.28
TR hub stationline	STA_{TR}	STATR	in.	520.7
TR hub waterline	WL_{TR}	WLTR	in.	118.27

TABLE J-1.- Continued.

Name	Algebraic symbol	Computer mnemonic	Units	Example value
Aircraft mass and inertia				
Aircraft weight	W_{ic}	WAITIC	lb	8000
Aircraft roll inertia	I_{XX}	XIXXIC	slug-ft^2	2700
Aircraft pitch inertia	I_{YY}	XIYYIC	slug-ft^2	12800
Aircraft yaw inertia	I_{ZZ}	XIZZIC	slug-ft^2	10800
Aircraft cross product of inertia	I_{YZ}	XIXZIC	slug-ft^2	950
Center of gravity stationline	$STA_{c.g.}$	STACG	in.	196
Center of gravity waterline	$WL_{c.g.}$	WLCG	in.	73
Center of gravity buttline	$BL_{c.g.}$	BLCG	in.	0
Fuselage (Fus)				
Fus aerodynamic reference point stationline	STA_{ACF}	STAACF	in.	200
Fus aerodynamic reference point waterline	WL_{ACF}	WLACF	in.	54
Fus drag, $\alpha = \beta = 0$	$\frac{D_0}{q}$	D1	ft^2	5.5
Fus drag, variation with α	$\frac{\partial(D/q)}{\partial\alpha}$	D2	ft^2/rad	-4.01
Fus drag, variation with α^2	$\frac{\partial^2(D/q)}{\partial\alpha^2}$	D3	ft^2/rad^2	41.56
Fus drag, variation with β^2	$\frac{\partial^2(D/q)}{\partial\beta^2}$	D4	ft^2/rad^2	141.16
Fus drag, $\alpha = 90°$	$\left.\frac{D}{q}\right\|_{\alpha=90}$	D5	ft^2	84.7
Fus drag, $\beta = 90°$	$\left.\frac{D}{q}\right\|_{\beta=90}$	D6	ft^2	156.1
Fus lift, $\alpha = \beta = 0$	$\frac{L_0}{q}$	XL0	ft^2	-4.11
Fus lift, variation with α	$\frac{\partial(L/q)}{\partial\alpha}$	XL1	ft^2/rad	15.64
Fus side force, variation with β	$\frac{\partial(Y/q)}{\partial\beta}$	Y1	ft^2/rad	93.85
Fus rolling moment, variation with β	$\frac{\partial(\ell/q)}{\partial\beta}$	YL1	ft^3/rad	246.31
Fus rolling moment, $\beta = 90°$	$\left.\frac{\ell}{q}\right\|_{\beta=90°}$	YL2	ft^3	0

TABLE J-1.- Continued.

Name	Algebraic symbol	Computer mnemonic	Units	Example value
Fus pitch moment, $\alpha = \beta = 0$	$\frac{M}{q}$	XM1	ft^3	-6.901
Fus pitch moment, variation with α	$\frac{\partial(M/q)}{\partial\alpha}$	XM2	ft^3/rad	280.405
Fus pitch moment, $\alpha = 90°$	$\left.\frac{M}{q}\right\|_{\alpha=90}$	XM3	ft^3	300
Fus yaw moment, variation with β	$\frac{\partial(N/q)}{\partial\beta}$	XN1	ft^3/rad	-913.35
Fus yaw moment, $\beta = 90°$	$\left.\frac{N}{q}\right\|_{\beta=90}$	XN2	ft^3	-600
Horizontal stabilizer (HS)				
HS station	STA_{HS}	STAHS	in.	398.5
HS waterline	WL_{HS}	WLHS	in.	56.0
HS incidence angle	i_{HS}	AIHS	rad	0
HS area	S_{HS}	SHS	ft^2	14.7
HS aspect ratio	AR_{HS}	ARHS	N-D	3.0
HS maximum lift curve slope	$C_{L_{max_{HS}}}$	CLMHS	N-D	1.2
HS dynamic pressure ratio	η_{HS}	XNH	N-D	0.8
Main rotor induced velocity effect at HS	$K_{V_{MR}}$	XKVMR	N-D	1.0
Vertical fin (VF)				
VF stationline	STA_{VF}	STAVF	in.	501
Vertical fin waterline	WL_{VF}	WLVF	in.	84
VF Incidence angle	i_{VF}	AIFF	rad	0
VF area	S_{VF}	SF	ft^2	18.6
VF aspect ratio	AR_{VF}	ARF	N-D	1.56
VF sweep angle	Λ_F	ALMF	rad	0.7853
VF maximum lift curve slope	$C_{L_{max_{VF}}}$	CLMF	N-D	1.2
VF dynamic pressure ratio	η_{VF}	VNF	N-D	0.9
Tail rotor induced velocity effect at VF	$k_{V_{TR}}$	XKVTR	N-D	0.9

TABLE J-1.- Concluded.

Name	Algebraic symbol	Computer mnemonic	Units	Example value
Controls				
Swashplate lateral cyclic pitch for zero lateral cyclic stick	$C_{A_{1_S}}$	CAIS	rad	0.0
Swashplate longitudinal cyclic pitch for zero longitudinal cyclic stick	$C_{B_{1_S}}$	CBIS	rad	0.0
Longitudinal cyclic control sensitivity	CK_1	CK1	rad/in.	0.03927
Lateral cyclic control sensitivity	CK_2	CK2	rad/in.	0.02618
Main rotor root collective pitch for zero collective stick	C_5	C5	rad	0.1501
Main rotor collective control sensitivity	C_6	C6	rad/in.	0.036652
Tail rotor root collective pitch for zero pedal position	C_7	C7	rad	0.11781
Pedal sensitivity	C_8	C8	rad/in.	0.08055

REFERENCES

1. Sinacori, J. B.; Stapleford, R. L.; Jewell, W. F.; and Lehman, J. M.: Researcher's Guide to the NASA Ames Flight Simulator for Advanced Aircraft (FSAA), NASA CR-2875, Aug. 1977.

2. Chen, R. T. N.: A Simplified Rotor System Mathematical Model for Piloted Flight Dynamics Simulation, NASA TM-78575, May 1979.

3. Chen, R. T. N.: Effects of Primary Rotor Parameters on Flapping Dynamics, NASA TP-1431, Jan. 1980.

4. Gessow, A.; and Meyers, Jr., G. D.: Aerodynamics of the Helicopter. Frederick Ungar Pub. Co. (New York), 1952.

5. Seckel, E.; and Curtiss, Jr., H. C.: Aerodynamic Characteristics of Helicopter Rotors. Dept. of Aerospace and Mechanical Eng. Rep. 659, Princeton Univ., 1962.

6. White, F.; and Blake, B. B.: Improved Method of Predicting Helicopter Control Response and Gust Sensitivity. Paper 79-25, 35th Ann. Nat. Forum of the AHS, Wash., D.C., May 1979.

7. Chen, R. T. N.: Selection of Some Rotor Parameters to Reduce Pitch-Roll Coupling of Helicopter Flight Dynamics. Preprint No. I-6, paper presented at the AHS National Specialist's Meeting on Rotor System Design, Philadelphia, Penn., Oct. 22-24, 1980.

8. Davis, J. M.; Bennett, R. L.; and Blankenship, B. L.: Rotorcraft Flight Simulation with Aeroelastic Rotor and Improved Aerodynamic Representation, Vol. 1 — Engineer's Manual, USAAMRDL-TR-74-10A, June 1974.

9. Military Specification, Flying Qualities of Piloted Airplanes, MIL-F-8785B(ASG), Aug. 1969.

10. Jewel, Jr., J. W.; and Heyson, H. H.: Charts of Induced Velocities Near a Lifting Rotor, NASA MEMO 4-15-59L, May 1959.

1. Report No. NASA TM-84281	2. Government Accession No.	3. Recipient's Catalog No.
4. Title and Subtitle A MATHEMATICAL MODEL OF A SINGLE MAIN ROTOR HELICOPTER FOR PILOTED SIMULATION		5. Report Date September 1982 6. Performing Organization Code
7. Author(s) Peter D. Talbot, Bruce E. Tinling, William A. Decker, and Robert T. N. Chen		8. Performing Organization Report No. A-9033 10. Work Unit No. T-6292Y
9. Performing Organization Name and Address NASA Ames Research Center Moffett Field, California 94035		11. Contract or Grant No.
12. Sponsoring Agency Name and Address National Aeronautics and Space Administration Washington, D.C. 20546		13. Type of Report and Period Covered Technical Memorandum 14. Sponsoring Agency Code

15. Supplementary Notes

Point of Contact: William A. Decker, Mail Stop 211-2, NASA Ames Research Center, Moffett Field, CA 94035 (415) 965-5362 or FTS 448-5362

16. Abstract

This report documents a helicopter mathematical model suitable for piloted simulation of flying qualities. The mathematical model is a non-linear, total force and moment model of a single main rotor helicopter. The model has ten degrees of freedom: six rigid-body, three rotor-flapping, and the rotor rotational degrees of freedom. The rotor model assumes rigid blades with rotor forces and moments radially integrated and summed about the azimuth. The fuselage aerodynamic model uses a detailed representation over a nominal angle of attack and sideslip range of ±15°, and it uses a simplified curve fit at large angles of attack or sideslip. Stabilizing surface aerodynamics are modeled with a lift curve slope between stall limits and a general curve fit for large angles of attack. A generalized stability and control augmentation system is described. Additional computer subroutines provide options for a simplified engine/governor model, atmospheric turbulence, and a linearized six-degree-of-freedom dynamic model for stability and control analysis.

17. Key Words (Suggested by Author(s))	18. Distribution Statement
Helicopter Flight simulation; Handling qualities Helicopter aerodynamics Helicopter flight dynamics Helicopter stability and control augmentation system	Unlimited Subject Category - 08

19. Security Classif. (of this report)	20. Security Classif. (of this page)	21. No. of Pages	22. Price*
Unclassified	Unclassified	55	A04

*For sale by the National Technical Information Service, Springfield, Virginia 22161